### nature communications



**Article** 

https://doi.org/10.1038/s41467-025-64255-8

# Loss of BPTF restores estrogen response and suppresses metastasis of mammary tumors

Received: 26 February 2025

Accepted: 11 September 2025

Published online: 15 October 2025



Michael F. Ciccone<sup>1,12</sup>, Dhivyaa Anandan  $\textcircled{0}^{1,2,3,12}$ , Deeptiman Chatterjee  $\textcircled{0}^{1,12}$ , Chen Chen<sup>4,12</sup>, Marygrace C. Trousdell  $\textcircled{0}^{5}$ , Rebecca Anderson  $\textcircled{0}^{1}$ , Steven M. Lewis  $\textcircled{0}^{1,2,3}$ , Mackenzie K. Callaway  $\textcircled{0}^{1}$ , Chris Z. Zhao<sup>1,6</sup>, Amritha Varshini Hanasoge Somasundara  $\textcircled{0}^{7}$ , Suzanne Russo<sup>1</sup>, Shih-Ting Yang  $\textcircled{0}^{1}$ , Yixin Zhao  $\textcircled{0}^{8}$ , Julie Ostrander  $\textcircled{0}^{9}$ , John E. Wilkinson<sup>10</sup>, William C. K. Pomerantz  $\textcircled{0}^{11}$ , Adam Siepel  $\textcircled{0}^{1}$ , David L. Spector  $\textcircled{0}^{1}$ , Jessica Tollkuhn  $\textcircled{0}^{1}$  & Camila O. dos Santos  $\textcircled{0}^{1}$ 

Context-specific epigenetic dependencies, shaped by chromatin remodeling can create exploitable vulnerabilities for cancer therapies that are unique to tissue types and cellular identities. Here, we show that loss of BPTF (Bromodomain PHD Finger Transcription Factor), a core component of the NURF (Nucleosome Remodeling Factor) complex, results in the emergence of estrogen-responsive, tamoxifen-sensitive, Estrogen Receptor alpha (ER $\alpha$ ) positive mammary tumors without altering cancer cell state and tumor pathology. Elevated ER $\alpha$  levels in BPTF<sup>KO</sup> mammary tumor cells are linked with decreased TGF- $\beta$  activity and limited metastatic spread of mammary tumor cells to the lungs. Loss of ER $\alpha$  is sufficient to restore TGF- $\beta$  activity and the metastatic potential in BPTF<sup>KO</sup> tumors. These findings highlight a mechanism through which BPTF regulates tumor development and progression in mammary epithelial cells, offering insights into the interplay between chromatin remodeling, estrogen signaling, and their resultant adjuvant therapeutic potential in breast cancer.

Among the various therapeutic targets being interrogated for their role and dependency in cancer development and progression, those associated with epigenetic factors have recently been of high interest since they operate within transcriptional regulatory cues that are often specific to cancer cells. To test the ability of epigenetic perturbations to suppress tumor development, the scientific community has leveraged in vitro and ex vivo genetic loss of function studies, genetically engineered pre-clinical models, and small molecule inhibitors of epigenetic factors. Through these studies, several epigenetic perturbations have been described to deprive cancer cells of their growth and

motility in several models of mammary carcinoma<sup>1-4</sup>. Yet, it is plausible to assume that assessing gross properties of the tumor, such as tumor size, can only partially inform the dependency of epigenetic factors in breast tumorigenesis. Therefore, understanding how perturbations to epigenetic factors modulate the expression of genes that define the identity of various cell populations within a tumor can reveal selective effects on tumor initiation, progression, and therapeutic resistance.

Endocrine therapies, such as tamoxifen (TAM), are a mainstay for treating Estrogen Receptor-positive (ER $\alpha$ +) breast cancers, which represent the most common type of breast cancer diagnosed in

<sup>1</sup>Cold Spring Harbor Laboratory, Cold Spring Harbor, NY, USA. <sup>2</sup>Graduate Program in Genetics, Stony Brook University, Stony Brook, NY, USA. <sup>3</sup>Medical Scientist Training Program, Stony Brook University, Stony Brook, NY, USA. <sup>4</sup>Washington University School of Medicine in St. Louis, St. Louis, MO, USA. <sup>5</sup>Center for Computational Molecular Biology, Brown University, Providence, RI, USA. <sup>6</sup>School of Biological Sciences, Cold Spring Harbor Laboratory, Cold Spring Harbor, NY, USA. <sup>7</sup>Human Oncology and Pathogenesis Program, Memorial Sloan Kettering Cancer Center, New York, NY, USA. <sup>8</sup>Yazhouwan National Laboratory, Sanya, Hainan, China. <sup>9</sup>Masonic Cancer Center, University of Minnesota, Minneapolis, MN, USA. <sup>10</sup>Department of Comparative Medicine, University of Washington, Seattle, WA, USA. <sup>11</sup>Department of Chemistry, University of Minnesota, Minneapolis, MN, USA. <sup>12</sup>These authors contributed equally: Michael F. Ciccone, Dhivyaa Anandan, Deeptiman Chatterjee, Chen Chen. ⊠e-mail: dossanto@cshl.edu

women. While endocrine therapies have been partially responsible for the drastic decrease in breast cancer-related mortality, resistance to endocrine therapies and the recurrence of breast cancer pose significant obstacles to their efficacy. Several mechanisms have been identified as drivers of endocrine therapy resistance and recurrence, including the persistence and outgrowth of endocrine therapyresistant subclones as well as alterations in transcription factor activity and lineage plasticity<sup>5,6</sup>. Given the importance of ERα activity and cell states in mediating susceptibility to endocrine therapies, there has been growing clinical interest in exploring the use of drugs targeting epigenetic modifiers to reprogram endocrine therapy-resistant cell states and enable greater therapeutic efficacy<sup>7,8</sup>. In this study, we demonstrate how loss of function of the epigenetic factor bromodomain PHD finger transcription factor (BPTF) drives alterations to the epigenome of breast cancer cells that simultaneously induce ERa expression, TAM sensitivity, and metastasis inhibition.

BPTF is the largest and essential subunit of the NURF chromatin remodeling complex<sup>9,10</sup>, known to form an alternative NURF complex with SMARCA5 and BAP18 in leukemia cells<sup>11</sup> and to play a major role in cMYC transcriptional regulation<sup>12</sup>. In the mammary gland, BPTF deletion has been shown to alter mammary epithelial stem cell (MaSC) proliferation, self-renewal, transcriptional output, and differentiation<sup>13</sup>. BPTF has also been implicated in regulating the survival of human breast cancer cell lines, and BPTF knockdown slows the progression of mammary tumors in vivo<sup>14,15</sup>. However, many of the molecular mechanisms of BPTF inhibition in governing cancer cell states, tumor heterogeneity, and disease progression are yet to be elucidated. To address this, we crossed an inducible BPTF loss-of-function mouse model<sup>13</sup> with the classic mammary tumorigenesis model, MMTV-PyMT<sup>16</sup>.

We found that loss of BPTF delayed the onset of mammary tumorigenesis and suppressed the development of lung metastasis. Single-cell RNA sequencing (scRNA-seq) of pre-malignant mammary tissue revealed enrichment of ER $\alpha$ -regulated transcriptional processes in BPTF-deficient epithelial cells, and tissue analysis further confirmed elevated ER $\alpha$  expression in BPTF<sup>KO</sup> mammary tumors. Organoid analyses revealed enhanced responsiveness to estrogen and increased expression of estrogen-regulated genes in BPTF<sup>KO</sup> tumor organoids. Consistently, loss of BPTF function restored sensitivity to TAM treatment in tumor organoid systems, human breast cancer cell lines, and in vitro and in vivo models characterized as resistant to endocrine therapy<sup>17</sup>.

Given that increased ERa protein levels have been reported to inhibit the metastatic spread of breast cancer cells by inhibiting TGF-β signaling<sup>18,19</sup>, we sought to determine whether ERα expression in BPTF<sup>KO</sup> mammary tumors played a role on suppressing the metastasis development observe in our model. To do so, we developed an MMTV-PyMT mammary tumorigenesis model bearing deletion of both Bptf and Esr1. Loss of ERα expression in BPTFKO cells restored TGF-β signaling activity and the metastatic potential of mammary tumor cells, shedding light on a mechanism in which BPTF collectively orchestrates hormone responses and metastatic progression during mammary oncogenesis. Furthermore, our studies also demonstrated that pharmacologic inhibition of BPTF with two distinct small-molecule inhibitors was sufficient to induce gain of ERα expression, sensitivity to TAM treatment, and inhibition of metastatic progression of hormonenegative mammary tumor models. Together, these findings highlight the strong potential of BPTF inhibition as a powerful and promising therapeutic avenue for activating ER\alpha expression and endocrine therapy responses in hormone-negative breast cancer.

#### **Results**

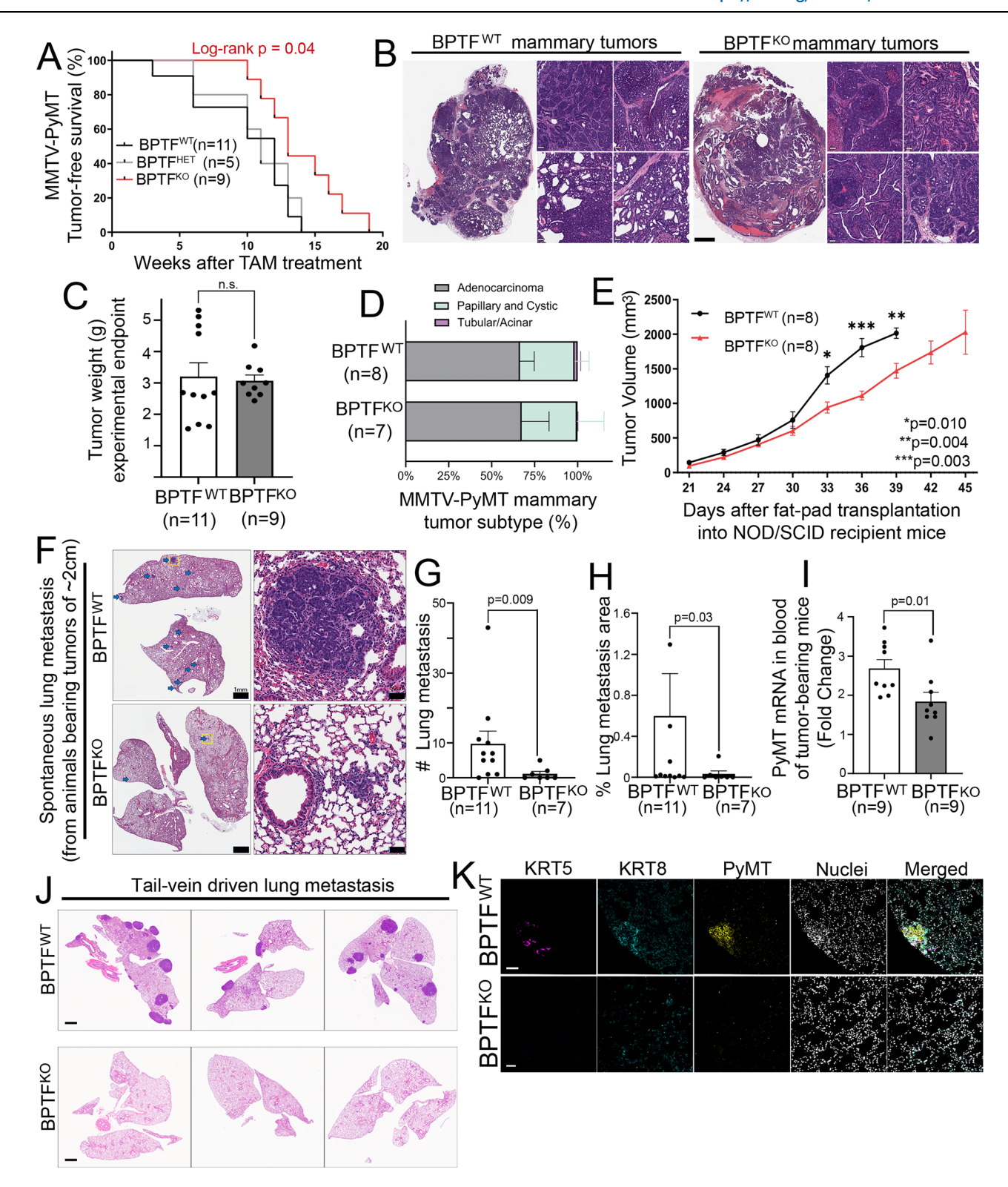
# Loss of BPTF alters initiation and metastatic development of mammary tumors

High levels of BPTF expression have been reported in several cancer types, including breast cancer<sup>20</sup>. Indeed, around 9% of the patients in

the Mercurio Laboratory Molecular Taxonomy of Breast Cancer International Consortium and The Cancer Genome Atlas invasive breast carcinoma cohorts (cbioportal.org) bear genetic alterations in the BPTF gene, which are associated with poor prognosis (Supplementary Fig. 1A-C)<sup>21-25</sup>. In agreement, analysis of patient-derived breast tumor tissue arrays confirmed ten-fold higher BPTF protein levels over normal breast tissue, thus supporting a link between high levels of BPTF and breast cancer (Supplementary Fig. 1D, E). CRISPR-based loss of function analysis indicated that BPTF depletion in human breast cancer cell lines impacted cell proliferation, an observation that corroborates previous studies that utilized either RNAi or small molecule chemical inhibitors<sup>20,26,27</sup> (Supplementary Fig. 1F, G). Yet, these studies did not elucidate the molecular mechanisms triggered by BPTF inhibition that impact cancer cell growth, nor did they inform the effects of BPTF loss of function during the early stages of breast cancer development and progression. Therefore, to address these unresolved questions, we crossed a spontaneous model of mammary tumorigenesis, MMTV-PyMT, with a TAM-inducible system previously shown to effectively delete BPTF from Cytokeratin 5 positive (Krt5+) normal mammary stem/progenitor cells<sup>13</sup>. Given that Krt5+ cells are also found in the mammary tumors and lung metastases from MMTV-PyMT models, this model allows for investigating the role of BPTF in both mammary tumor initiation and progression (Supplementary Fig. 2A). mRNA and protein analysis confirmed reduced BPTF levels in BPTF<sup>KO</sup> tumor cells (Supplementary Fig. 2B, C and Supplementary Table 1).

Tumor-free survival analysis demonstrated a significant delay in tumor onset after BPTF deletion, with 100% of BPTF<sup>KO</sup> mice being tumor-free 10 weeks post TAM-treatment, in contrast to 50% of BPTF<sup>WT</sup> and BPTF<sup>HET</sup> mice bearing tumors 10 weeks post TAM-treatment (Fig. 1A, B). As a result of delayed tumor initiation, BPTF<sup>KO</sup> mice reached maximum tumor burden seven weeks after BPTF<sup>WT</sup> and BPTF<sup>HET</sup> mice. Further analysis of mammary tumors at endpoint demonstrated that BPTF<sup>WT</sup> and BPTF<sup>KO</sup> mice developed tumors with similar size spanning the histological subtypes commonly observed in the MMTV-PyMT model (adenocarcinoma, papillary and tubular/acinar), thus suggesting that while BPTF loss delayed tumor onset, it did not alter the histopathological features of mammary tumors (Fig. 1C, D).

Mammary tumor development is heavily influenced by the immune microenvironment, with certain populations of immune cells, such as T cells and NK cells, playing a putative role in inhibiting tumor growth<sup>28,29</sup>. In fact, previous reports showed that RNAi-knockdown of BPTF in a syngeneic mouse breast cancer models mildly impacted tumor growth and stimulated the infiltration of cytotoxic NK cells into frank tumors<sup>30</sup>. Therefore, we next tested whether the delayed tumor onset in BPTF<sup>KO</sup> mice was a consequence of changes in the mammary immune microenvironment. To do so, we utilized a cell transplantation approach, where non-TAM-treated MMTV-PyMT Krt5<sup>Cre-ERT2</sup>Bptf fl/fl mammary tumor cells (BPTFWT) were injected into the mammary fat pad of immunodeficient NOD/SCID female mice. NOD/SCID recipient mice were then either TAM-treated to induce BPTF deletion in mammary tumor cells or treated with oil as a control. Our analysis indicated that even in immunodeficient conditions. BPTF<sup>KO</sup> mammary tumors grew slower, reaching maximum tumor burden around 45 days, in contrast to BPTFWT tumors, which reached maximum tumor burden by day 35 (Fig. 1E). This suggests that loss of BPTF in MMTV-PyMT tumor cells impacts mammary tumorigenesis even in an immunodeficient microenvironment. We also performed flow cytometry analysis of BPTFWT and BPTFKO tumors harvested from immunocompetent mice and NOD/SCID mice to characterize the tumor immune microenvironment in these models. Our flow cytometry analysis did not identify changes in the abundance of macrophages (CD11b+, CD206+), neutrophils (CD11b+, Ly6G+), dendritic cells (CD11c+, CD103+), NK cells (CD3-, NK1.1+), or T cells (CD3+) in tumors from immunocompetent mice, and the same trends in the abundance of macrophages, neutrophils, dendritic cells, and NK cells were observed for



tumors from NOD/SCID mice (Supplementary Fig. 2D–F). These results further corroborate the notion that delayed tumor onset in response to loss of BPTF is likely driven by epithelial cell-intrinsic changes.

To characterize the effect of BPTF loss in later stages of mammary oncogenesis, we next set out to investigate whether BPTF loss of function affected metastatic progression. To do so, we harvested and analyzed lung tissue from tumor-bearing MMTV-PyMT BPTF<sup>WT</sup> and BPTF<sup>KO</sup> mice at experimental end point (tumor size for both genotypes -2 cm). We found that lung tissue from BPTF<sup>KO</sup> animals displayed an 8.5-fold decrease in the number of metastatic foci and an 18-fold

decrease in the size of the metastatic foci compared to those observed in BPTF<sup>WT</sup> animals (Fig. 1F–H). As a surrogate for detecting circulating tumor cells, we analyzed *PyMT* mRNA levels in the blood from mice bearing either BPTF<sup>WT</sup> or BPTF<sup>KO</sup> tumors (similar size at endpoint). qPCR for *PyMT* mRNA indicated a two-fold decrease in *PyMT* mRNA in the blood of mice transplanted with BPTF<sup>KO</sup> tumor cells (Fig. 1I and Supplementary Table 1).

Although lung metastases were evaluated at a time point when BPTF<sup>WT</sup> and BPTF<sup>KO</sup> animals had similar tumor size, the delayed onset of the primary mammary tumor formation in BPTF<sup>KO</sup> mice could affect

# **Fig. 1** | **Loss of BPTF** alters initiation and metastatic development of mammary tumors. **A** Tumor-free survival analysis of BPTF<sup>WT</sup> (black line n=11), BPTF<sup>HET</sup> (gray line n=5), and BPTF<sup>KO</sup> MMTV- PyMT mice (red line n=9). Statistical analysis performed with Log-rank (Mantel–Cox) test (two-tailed). **B** H&E-stained histological images of mammary tumors from BPTF<sup>WT</sup> (left panels) and BPTF<sup>KO</sup> (right panels), Scale bar = 1 mm. Zoom-in panels, Scale bar = 50 $\mu$ m. **C** Wet weight (in grams) of BPTF<sup>WT</sup> (black bar n=11) and BPTF<sup>KO</sup> (red line n=9) mammary tumors at experimental endpoint (-2 cm). **D** Histopathological classification of mammary tumors from BPTF<sup>WT</sup> and BPTF<sup>KO</sup> mice. **E** Tumor growth (in mm³) of NOD/SCID mice transplanted with either BPTF<sup>WT</sup> or BPTF<sup>KO</sup> tumor cells. **F** H&E-stained histological images from the lungs from BPTF<sup>WT</sup> (top panels) and BPTF<sup>KO</sup> (bottom panels) mice (at experimental end point, tumors -2 cm), with arrows indicating metastatic lesions. Scale bar = 1 mm. Zoom-in panels, Scale bar = 50 $\mu$ m. **G** Quantification of the number of metastatic lung lesions in BPTF<sup>WT</sup> (n=11) and BPTF<sup>KO</sup> (n=7) tumor-bearing female mice (at experimental end point, tumors -2 cm). **H** Quantification of

the area of metastatic lung lesions in BPTF<sup>WT</sup> (n = 11) and BPTF<sup>KO</sup> (n = 7) tumorbearing female mice (at experimental end point, tumors -2 cm). I Quantification of PyMT mRNA levels in the peripheral blood of tumor-bearing C57BL/6 transplanted (fatpad) with BPTF<sup>WT</sup> (n = 9) or BPTF<sup>KO</sup> (n = 9) mammary tumor cells (at experimental end point, tumors -2 cm). J H&E-stained histological images from the lungs of C57BL/6 female mice that were injected (tail vein) with either BPTF<sup>WT</sup> (top panels) or BPTF<sup>KO</sup> (bottom panels) primary mammary tumor cells. Scale bar = 1 mm. **K** IF analysis of lung tissue from C57BL/6 mice tailed-injected with BPTF<sup>WT</sup> or BPTF mammary tumor organoid cells, showing metastatic cells stained for KRT5 (magenta), KRT8 (cyan), and PyMT (yellow) proteins. Nuclei (DAPI) = gray. Scale bar = 100  $\mu$ m. Statistical analysis performed with an unpaired t-test with Welch's correction (two-sided), and differences were considered significant if p < 0.05. Error bars represent standard error mean. Samples (n) represent number of individual mice or number biological replicates. Raw data and p values are provided as a Source Data file.

the kinetics of tumor cell dissemination, consequently affecting the establishment of lung metastasis. Therefore, we next decided to parse out whether BPTF loss specifically affects the colonization of the lung by delivering BPTFWT and BPTFKO MMTV-PyMT tumor cells intravenously (tail vein), thereby bypassing the tumor cell extravasation step of the metastatic cascade (Supplementary Fig. 3A). Histological analysis of the lungs from these mice identified a ten-fold decrease in the number of lung metastasis lesions in mice injected with BPTF<sup>KO</sup> tumor cells, thus demonstrating that BPTF<sup>KO</sup> cells are not able to colonize the lungs of mice as efficiently as BPTFWT tumor cells, even when introduced directly into the circulation (Fig. 1J, K and Supplementary Fig. 3B). This finding was supported by a substantial decrease in *PyMT* mRNA levels detected in the lungs of tail vein-injected mice (Supplementary Fig. 3C and Supplementary Table 1). To investigate the effects of BPTF deletion on tumor cell migration independent of the influence of surrounding stroma and immune cells, we generated mammary organoid cultures from BPTFWT and BPTFKO endpoint MMTV-PyMT tumors. Organoids derived from BPTFWT and BPTFKO displayed similar cell cycle staging, indicating that once developed, both tumor cell models adapted well to ex vivo growth conditions (Supplementary Fig. 3D). Using these organoid systems, we further tested the effects of BPTF loss on the metastatic properties of mammary tumor cells. Using a 3D Matrigel drop invasion assay, we found that BPTF<sup>KO</sup> organoids occupied less migration area compared to BPTFWT organoids, indicating decreased migratory potential induced by BPTF loss (Supplementary Fig. 3E, F). We also performed a Transwell migration assay on BPTFWT and BPTFKO tumor organoids and saw that fewer BPTFKO tumor cells migrated to the bottom chamber of the Transwell, further alluding to the defective overall metastatic ability of tumor cells associated with the loss of BPTF (Supplementary Fig. 3G, H).

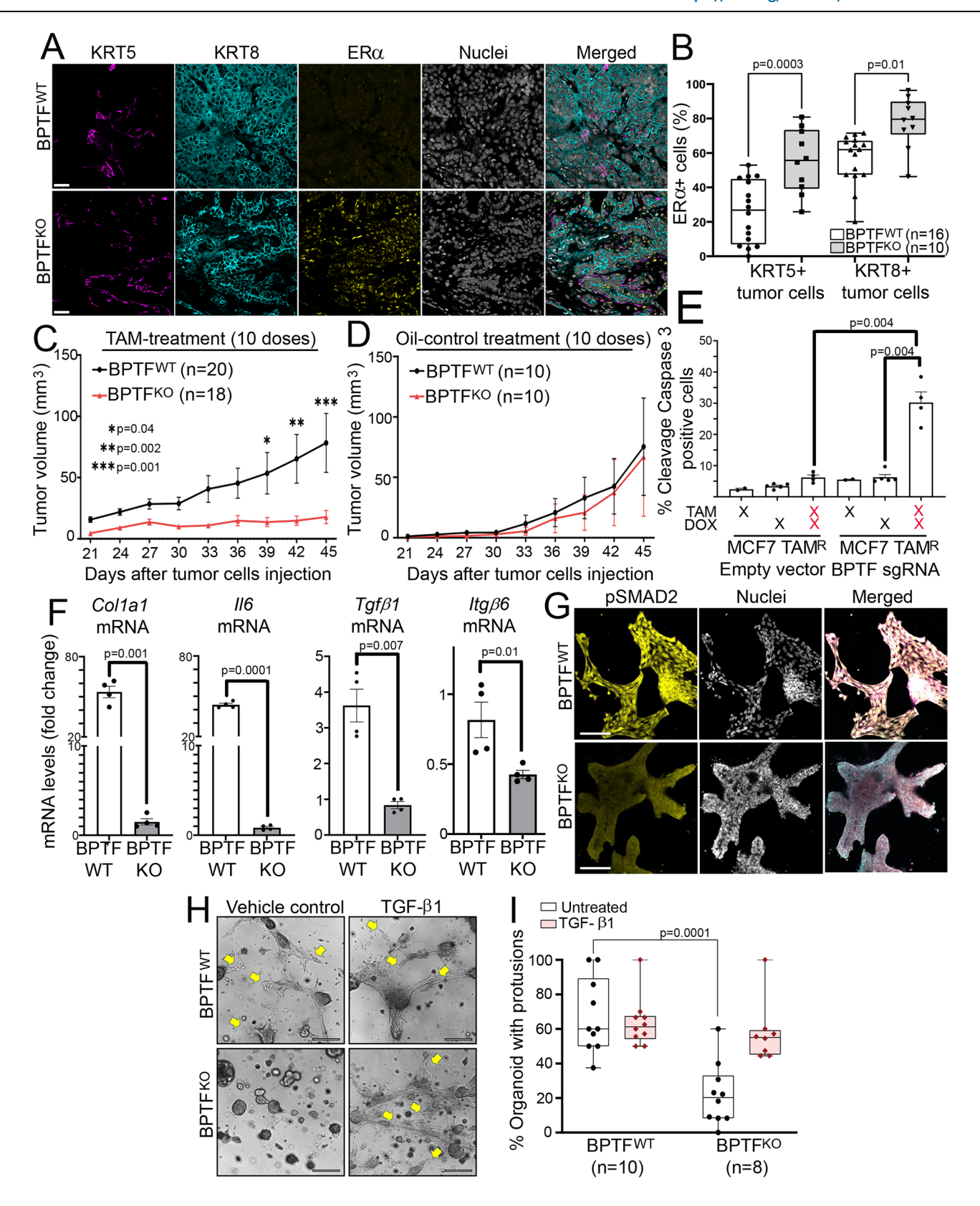
# Loss of BPTF enhances $\text{ER}\alpha$ protein expression in MMTV-PyMT mammary tumors

We next set out to identify the molecular perturbations induced by BPTF loss of function that delayed the onset of mammary tumorigenesis and inhibited the development of lung metastasis. To do so, we generated scRNA-seq profiles of MMTV-PyMT BPTFWT and BPTFKO mammary tissue three weeks post-TAM treatment, a timepoint prior to the detection of palpable tumors that was selected to capture the initial stages of mammary tumorigenesis (Supplementary Table 2). Analysis of mammary Epcam+ cells from non-tumor-bearing BPTFWT and BPTFKO mice identified all three major mammary epithelial cell types, including Luminal progenitor-like cells (LASP, clusters C1, C2, C3, C5, C7, and C11), Luminal Hormone sensing cells (LHS, clusters C4, C8, C10, and C12), and Basal-Myoepithelial cells (BMyo, clusters C6 and C9), according to the expression of previously described lineage signatures<sup>31</sup> (Supplementary Fig. 4A, B). Statistical analysis of cell type proportions using Propeller<sup>32</sup> did not indicate statistically significant changes to the abundance of cells within each cluster, suggesting that the epithelial composition was comparable between BPTF<sup>WT</sup> and BPTF<sup>KO</sup> mammary tissue prior to tumor onset.

Further analysis of differentially expressed genes (DEGs) and gene set enrichment analysis across BMvo clusters indicated the gain of Estrogen regulatory pathways in BPTFKO myoepithelial cells prior to tumor development (Supplementary Fig. 4C). This enrichment in estrogen-regulated pathways was linked with the overall gain of Esr1 mRNA in all epithelial cells, with BMyo cells having the greatest increase in Esr1 mRNA levels (Supplementary Fig. 4D). In fact, further analysis of all BPTFKO cells indicated an enrichment for Estrogendependent gene expression across all clusters (Supplementary Fig. 4E). Interestingly, increased Esr1 mRNA levels were also observed in BPTF<sup>HET</sup> mammary epithelial cells from wildtype C57BL/6 (non-MMTV-PyMT mice) (Supplementary Fig. 4F, G). This observation agrees with previous reports, which showed increased mRNA levels of luminalspecific genes in cell types specifically found in the mammary tissue after BPTF deletion<sup>13</sup>, and collectively suggesting a role for BPTF in negatively regulating ERα in non-malignant mammary epithelial cells.

Tumors that develop from the MMTV-PvMT model start as ER $\alpha$ +. yet ERα expression declines as the cancer lesions advance into mid-tolate-stage disease<sup>33</sup>. Given our observation that loss of BPTF is accompanied by a gain of ERα-associated gene regulation prior to the formation of palpable mammary tumors, we next decided to investigate how ERa levels are affected in late-stage BPTFKO tumors. Immunofluorescent (IF) staining analysis of endpoint tumors demonstrated that BPTF $^{\text{KO}}$  mammary tumors displayed ~40% more ER $\alpha$ + tumor cells than tumors from BPTFWT mice, strengthening the link between the loss of BPTF function and increased  $ER\alpha$  expression that is sustained throughout mammary tumor progression (Fig. 2A, B). The net gain of ERα signal was greater in KRT5+ cells (Basal) than in KRT8+ cells (Luminal), an observation that supports the gain of ER $\alpha$  in BPTF $^{KO}$  nonluminal cells. Analysis of liver tissue did not identify increased  $ER\alpha$ protein levels in response to BPTF loss of function, suggesting that ERa activation was specific to mammary tissue (Supplementary Fig. 4H). qPCR and Western blot analysis of tumor organoid cultures confirmed that BPTFKO cells have a 2000-fold increase in Esr1 mRNA levels and over three-fold increase in ERa protein levels compared to BPTFWT cells, further validating that loss of BPTF function results in increased ERα expression in mammary tumor cells (Supplementary Fig. 5A, B and Supplementary Table 1).

ERα protein expression defines luminal hormone-sensing cell states, given their ability to activate cell proliferation in response to the ligand β-estradiol. Therefore, to test whether BPTF loss results in the gain of functional ERα, we utilized a previously characterized treatment protocol<sup>34</sup> and measured BPTF<sup>WT</sup> and BPTF<sup>KO</sup> mammary tumor organoid growth in response to β-estradiol supplementation compared to tumor organoids grown in normal growth media containing FGF2 (control). We found that the size of BPTF<sup>KO</sup> tumor organoids increased two-fold in response to β-estradiol (β-E<sub>2</sub>) treatment, which



did not occur in  $\beta$ -E<sub>2</sub>-treated BPTF<sup>WT</sup> tumor organoids (Supplementary Fig. 5C). These analyses indicate that BPTF<sup>KO</sup> tumor organoids, which express higher levels of ER $\alpha$ , are more responsive to estradiol treatment.

Due to the loss of ER $\alpha$  during tumor progression, MMTV-PyMT mammary tumors become resistant to TAM treatment, a commonly used treatment strategy for ER $\alpha$ + breast cancer<sup>35</sup>. Given that loss of

BPTF sustained the expression of ER $\alpha$  in MMTV-PyMT tumors, we next tested whether BPTF<sup>KO</sup> tumor cells also regained sensitivity to TAM, a therapy targeting ER $\alpha$ , ex vivo and in vivo. We first treated BPTF<sup>WT</sup> and BPTF<sup>KO</sup> mammary tumor organoid cultures with 4-hydroxytamoxifen (4-OHT), the active TAM metabolite, for 10 days and then analyzed organoid size. Our analysis indicated a two-fold decrease in the size of BPTF<sup>KO</sup> mammary tumor organoids in response to 4-OHT treatment,

Fig. 2 | Loss of BPTF enhances ERα protein expression in MMTV-PyMT mammary tumors. A Immunofluorescence (IF) images of BPTFWT and BPTFKO primary mammary tumors, showing KRT5 (magenta), KRT8 (cyan), ERα (yellow), Nuclei (DAPI, gray). Scale bar = 100 µm. **B** Box-and-whisker plot for the quantification of ER $\alpha$ + cells in KRT5+ and KRT8+ populations of BPTF<sup>WT</sup> (n = 16) and BPTF<sup>KO</sup> (n = 10) mammary tumors. The whiskers represent range of data distribution, center line is the median and the box represents the interquartile range (minimum-centermaximum values for each sample, from left-to-right are as follows: 0-26.79-52.94, 25.81-55.67-80.85, 20.08-61.89-71.49 and 46.21-79.61-96.34). C Tumor growth quantification (in mm<sup>3</sup>) of C57BL/6 female mice transplanted with either BPTFWT (n = 20 individual transplants) or BPTF<sup>KO</sup> (n = 18 individual transplants) mammary tumor organoids, and treated with TAM (100 µg/day, 10 doses). D Tumor growth quantification (in mm<sup>3</sup>) of C57BL/6 female mice transplanted with either BPTFWT (n = 10 individual transplants) or BPTF<sup>KO</sup> (n = 10 individual transplants) mammary tumor organoids, and treated with Oil (no TAM control, 100 µL/day, 10 doses). E Cleaved Caspase 3/7 activity of Empty Vector or BPTF sgRNA MCF7-TAMR cells treated with doxycycline (to induce BPTF editing), Tamoxifen or both. Since the MCF7-Tam<sup>R</sup> cells grow slowly and therefore are limited by cell numbers, individual

wells were combined to pool the cells. n = 4 experimental repeats per condition. **F** Quantification of *Col1a1*, *Il6*,  $Tgf\beta1$ , and  $Itg\beta6$  mRNA levels in BPTF<sup>WT</sup> and BPTF<sup>KO</sup> PyMT tumor organoids. n = 4 mammary tumor organoids derived from individual mammary tumors/animals. G Immunofluorescence (IF) images of BPTFWT and BPTFKO PyMT tumor organoids showing pSMAD2 (yellow), Nuclei (DAPI, gray) Scale bar = 100 µm. Representative images (H) and box-and-whisker plot for the quantification (I) of collagen I cell protrusion analysis of BPTFWT (n=10) and BPTFKO (n=8)organoids, treated with Vehicle control or TGF-β1 (2 ng/mL). Yellow arrows indicate organoid protrusions. The whiskers represent range of data distribution, center line is the median and the box represents the interquartile range (minimum-centermaximum values for each sample, from left-to-right are as follows: 37.5-60-100, 0-20.20-60, 50-61.25-100 and 44.44-55.05-100). Scale bar =  $100 \, \mu m$ . Statistical analysis was performed with a two-tailed, unpaired t-test with Welch's correction (two-sided) and no adjustments were made for multiple comparisons. For the statistical comparison shown in (I), non-parametric unpaired t-test (two-sided) was performed. Differences were considered significant if p < 0.05. Error bars represent standard error mean. Samples (n) represent number of individual mice or number biological replicates. Raw data and p values are provided as a Source Data file.

thus suggesting increased sensitivity to TAM (Supplementary Fig. 5D). We also tested whether the increased sensitivity to TAM was observed in vivo. To do so, we transplanted BPTF<sup>WT</sup> and BPTF<sup>KO</sup> mammary tumor cells into the fat pad of immunocompetent C57BL/6 mice. Starting one week after transplant, we treated the recipient mice with oil (control) or TAM for 10 days using an established treatment protocol<sup>17</sup> and measured tumor growth (Supplementary Fig. 5E). Mice that were transplanted with BPTF<sup>KO</sup> tumor cells and were treated with TAM failed to develop large tumors in comparison to TAM-treated mice that received BPTF<sup>WT</sup> cells (Fig. 2C). Conversely, oil-treated (no TAM control) mice transplanted with BPTF<sup>WT</sup> or BPTF<sup>KO</sup> demonstrated comparable tumor growth (Fig. 2D). All together, these analysis support that BPTF loss of function induces, likely due to increased ERα expression, are more sensitive to TAM treatment.

We next asked whether BPTF inhibition would restore sensitivity to human breast cancer cells that have acquired TAM resistance. To do so, we utilized a modified MCF-7 cell line designed to be resistant to TAM in vitro (referred hereafter as MCF-7 TAM<sup>R</sup>). Like the parental cell line. DOX-inducible targeting of BPTF with CRISPR-Cas9 progressively decreased the proliferation of MCF-7 TAM<sup>R</sup> cells, a phenotype that was marked by increased ESR1 mRNA levels due to BPTF loss (Supplementary Figs. 1F and 5F, J). In fact, simultaneous BPTF targeting (DOX treatment, p1) and TAM treatment resulted in a six-fold increase in apoptotic cells (cleavage caspase 3+) in comparison to MCF-7 TAM<sup>R</sup> cells that were either only treated with TAM or CRISPR-targeted BPTF, suggesting that loss of BPTF restored TAM sensitivity in vitro (Fig. 2E). BPTF deletion also increased ESR1 mRNA levels and TAM sensitivity of the hormone-negative human breast cancer cell line HCC-1143, thus demonstrating that, independent of the clinical subtype, loss of BPTF function drives the gain of ERa, increased response to estrogen, and increased sensitivity to TAM treatment (Supplementary Fig. 5H, I).

We next set out to determine the molecular basis of the inhibition of lung metastasis seen with BPTF loss. Considering previous reports that cancer cells with metastatic potential arise early during tumorigenesis<sup>36</sup>, we first set out to identify putative metastatic cells in our MMTV-PyMT BPTF<sup>WT</sup> scRNA-seq dataset. We found stronger expression of a metastasis-associated gene signature<sup>37</sup> in cluster C5 and in clusters C10 and C11, which are less abundant (Supplementary Figs. 4A, 6A and Supplementary Table 2). Further gene set enrichment analysis of cluster C5 between BPTF<sup>WT</sup> and BPTF<sup>KO</sup> conditions revealed a downregulation of pathways associated with cell polarity, interferon response, and epithelial-mesenchymal transition (EMT) in BPTF<sup>KO</sup> cells, which are all pathways that have previously been described to play a role in metastasis<sup>38-40</sup> (Supplementary Fig. 6B). Additional gene expression analysis comparing all BPTF<sup>WT</sup> and BPTF<sup>KO</sup> cell clusters indicated low expression of Serpin family E member 1 (*Serpine1*), SMAD

family member 3 (*Smad3*), and SMAD family member 6 (*Smad6*), which are all genes that are regulated by the Transforming Growth Factor  $\beta$  (TGF- $\beta$ ), a master regulator of proliferation, EMT, and metastatic progression of cancer cells<sup>41-43</sup> (Supplementary Fig. 6C). Down-regulation of genes downstream of TGF- $\beta$ , including Collagen type 1  $\alpha$ 1 (*Col1a1*), Interleukin 6 (*Il6*), Transforming growth factor  $\beta$ 1 (*Tgf\beta1*), and Integrin  $\beta$ 6 (*Itgb6*) was also observed in BPTF<sup>KO</sup> tumor organoids, thus further suggesting that BPTF loss dampens transcriptional programs related to TGF- $\beta$  activity and metastasis in mammary cancer cells (Fig. 2F and Supplementary Table 1).

Analysis of fibroblast populations prior to tumor development revealed similar distributions of myofibroblasts, immune-related fibroblasts, and collagen-related fibroblasts in both BPTFWT and BPTF<sup>KO</sup> mammary tissues (Supplementary Fig. 6D, E). This suggests that the inhibition of TGF-β programs in BPTF<sup>KO</sup> mammary tumor cells is likely to be intrinsic to epithelial cancer cells rather than being directly influenced by alterations in stromal composition that could serve as a source of TGF-β. In fact, ELISA protein analysis indicated a substantial decrease of TGF-B levels in the media from BPTFKO mammary organoids (8000-fold), or in the lysates from total mammary tumors (four-fold), compared to BPTFWT conditions (Supplementary Fig. 6F, G). In agreement, using IF staining analysis, we found a marked decrease in the nuclear localization of the phosphorylated form of the transcription factor SMAD2 (pSMAD2), the main signal transducer of TGF-β pathways, in BPTF<sup>KO</sup> tumor organoids (Fig. 2G). Collectively, our findings support that loss of BPTF results in the suppression of TGF-β molecular pathways and suggest that inhibition of such programs could influence the metastatic potential of BPTFKO mammary tumor cells.

To further confirm the role of TGF-β in mediating the migratory cell behavior of BPTF<sup>KO</sup> mammary tumor cells, we treated BPTF<sup>WT</sup> and BPTF<sup>KO</sup> mammary tumor organoids with TGF-β1 using a concentration previously shown to induce TGF-β molecular pathways. Using this strategy, we measured the development of cellular protrusions, which is an established readout of metastatic potential. Our analysis showed that BPTF<sup>KO</sup> organoids develop fewer cellular protrusions compared to BPTF<sup>WT</sup> organoids when they are not supplemented with TGF-β1, corroborating our in vivo results showing that BPTF loss inhibits metastasis. Notably, treatment of BPTF<sup>KO</sup> tumor organoids with TGF-β1 rescued cellular protrusion to nearly the same level as that seen in untreated or TGF-β1-treated BPTFWT tumor cells (Fig. 2H, I). Increased cellular protrusions were not observed in BPTFWT tumor organoids treated with TGF-β1. In agreement, treatment of BPTF<sup>KO</sup> mammary organoids with TGF-\(\beta\)1 also resulted in increased mRNA levels of several genes regulated by TGF-β, including Vimentin (Vim), Fibronectin (Fn1), Col1a1, Il6, and Tgf\(\beta\)1 (Supplementary Fig. 6H and

Supplementary Table 1). The cell protrusion phenotype was not rescued in BPTF<sup>KO</sup> tumor organoid cultures treated with Interleukin 1 $\beta$  (IL-1 $\beta$ ) or Tumor Necrosis Factor  $\alpha$  (TNF- $\alpha$ ), additional known regulators of metastatic cellular processes<sup>44,45</sup>, further pointing to TGF- $\beta$  as the key regulator of differences in metastatic features seen with BPTF loss (Supplementary Fig. 6I, J).

Collectively, these findings suggest that the loss of BPTF disrupts the acquisition of metastatic traits in tumor cells through TGF- $\beta$  molecular pathways, a phenotype that can be reversed with exogenous TGF- $\beta$ 1. These results imply that gene regulatory mechanisms in BPTF mammary tumor cells overrule the induction of EMT programs in response to naturally occurring levels of TGF- $\beta$  levels during mammary tumorigenesis.

#### 

Increased ER $\alpha$  protein levels have been reported to block the metastatic spread of breast cancer cells by inhibiting TGF- $\beta$  signaling through transcriptional and non-transcriptional mechanisms<sup>18,19</sup>. Therefore, we next set out to investigate whether the functional gain of ER $\alpha$  induced by BPTF loss underpins the molecular basis of the inhibition of TGF- $\beta$  signaling and lung metastasis.

Considering the role of BPTF as a putative chromatin remodeler, we first investigated the effects of BPTF inhibition on chromatin accessibility by performing ATAC-seq analysis in MCF-7 cells expressing sgRNA targeting BPTF<sup>46</sup> (Supplementary Table 2). We found that targeting BPTF with CRISPR-Cas9 results in the expansion of the accessible chromatin landscape in MCF-7 cells, including a three-fold increase in the ATAC-seq signal at estrogen response elements (EREs), which are canonical sites preferentially bound by ER $\alpha$  (Supplementary Fig. 7A–C). We also found a fifty-fold increase in *ESR1* mRNA levels in MCF-7 cells expressing BPTF sgRNA, once again supporting that the loss of BPTF function enhances ER $\alpha$  expression, and the accessibility of chromatin at regions predicted to be occupied by ER $\alpha$  (Supplementary Fig. 7D and Supplementary Table 1).

To determine whether ER $\alpha$  gain of function translated into transcriptional activation, we measured mRNA levels of three ERaregulated genes: the ENY2 transcription and export complex 2 subunit (Eny2), a gene associated with estrogen-regulated ductal outgrowth<sup>47</sup>, the Transcription factor AP-2β (*Tfap2b*), a factor known to induced Esr1 expression via epigenetic chromatin modification<sup>48</sup>, and the GATA binding protein 3 (Gata3), a known downstream target of ERa49. qPCR analysis of tumor-derived organoids revealed significantly elevated expression of all three genes in BPTF<sup>KO</sup> compared to BPTFWT samples (Fig. 3A and Supplementary Table 1). These findings support a link between ERα increased expression and transcriptional levels of key developmental regulators. To determine whether ERa expression is the main driver of tumor development, metastasis progression, and gene expression changes observed in BPTFKO mammary tumor epithelial cells, we generated an additional transgenic mouse model by crossing the MMTV-PyMT-Krt5<sup>CRE-ERT2</sup>-Bptf<sup>fl/fl</sup> with an Esr1<sup>fl/fl</sup> mouse model<sup>50</sup>. This strategy resulted in a model of MMTV-PyMT mammary tumorigenesis in which TAM treatment induced the deletion of both Bptf and Esr1. Interestingly, Bptf<sup>fl/fl</sup>/Esr1<sup>fl/fl</sup> female mice did not survive for more than three days after TAM treatment, indicating that the simultaneous loss of ERα and BPTF in Krt5+ cells was lethal in adult female mice (Supplementary Fig. 8A). Conversely, mortality was not observed in Bptf<sup>fl/fl</sup>/Esr1<sup>fl/fl</sup> male mice after TAM treatment. Therefore, to characterize the dynamics of tumor and metastasis development after BPTF and ERα loss, we performed mammary fat pad injections of endpoint tumors from non-TAM-treated MMTV-PyMT-Krt5<sup>CRE-ERT2</sup>-Bptf<sup>fl/fl</sup> (BPTF<sup>KO</sup>/ERα<sup>WT</sup>) or MMTV-PyMT-Krt5<sup>CRE-ERT2</sup>-Bptf<sup>fl/fl</sup>/ *Esr1*<sup>fl/fl</sup> (BPTF<sup>KO</sup>/ERα<sup>KO</sup>) into female C57BL/6 recipient mice. Seven days after transplant, mice were injected with TAM to induce the loss of BPTF or the loss of both BPTF and ERα (Supplementary Fig. 8B).

Tumor-free survival analysis demonstrated a significantly earlier onset of tumor development in mice with BPTFKO/ERQKO mammary tumors, in comparison to those with BPTF<sup>KO</sup>/ERα<sup>WT</sup> mammary tumors (Fig. 3B). Endpoint mammary tumors from both conditions had similar size (Supplementary Fig. 8C). BPTF<sup>KO</sup>/ERα<sup>KO</sup> mammary tumors also lacked ER $\alpha$  protein levels, confirming successful knockout of ER $\alpha$  in this model (Supplementary Fig. 8D). Interestingly, we found a six-fold increase in the number of metastatic foci in the lungs of BPTFKO/ERQKO tumor-bearing mice, suggesting that loss of ERa expression restored the metastatic potential of BPTFKO cancer cells (Supplementary Fig. 8E). Analysis of lungs from wildtype C57BL/6 injected via tail vein with either BPTF<sup>WT</sup>, BPTF<sup>KO</sup>/ERα<sup>WT</sup>, or BPTF<sup>KO</sup>/ERα<sup>KO</sup> mammary tumor cells indicated a three-fold increase in the levels of PyMT mRNA in animals injected with BPTFKO/ERaKO tumor cells, further supporting that loss of ERα expression restored the metastatic potential of BPTF<sup>KO</sup> cancer cells (Supplementary Fig. 8F and Supplementary Table 1).

Given that our previous analyses identified alterations in the TGFβ molecular pathway being associated with the metastatic inhibition of BPTFKO mammary tumor cells, we next investigated whether the loss of ERα in BPTFKO tumor cells was linked to the restoration of TGF-β activity. IF analysis indicated that loss of ER $\alpha$  was sufficient to restore the nuclear localization of pSMAD2 and in BPTFKO mammary tumor cells, supporting the notion that elevated ER $\alpha$  levels can inhibit the TGF-β pathway in the BPTF loss (Supplementary Fig. 8G, H). In agreement, loss of ERα also resulted in the upregulation of the TGF-β downstream genes Col1a1, Il6, and Tgfb1 in BPTFKO tumor cells, thus further linking the rescue of metastatic potential with the reestablishment of TGF-\( \beta \) signaling (Fig. 3C). We also found decreased mRNA levels of the BPTF<sup>KO</sup>- ER $\alpha$ -bound genes *Tfap2\beta* and *Gata3* in BPTF<sup>KO</sup>/ERα<sup>KO</sup> tumor cells compared to BPTF<sup>KO</sup>/ERα<sup>WT</sup> tumor cells, confirming the role of  $\text{ER}\alpha$  in inducing the transcription of these genes in the context of BPTF loss (Fig. 3D and Supplementary Table 1). Taken together, these results support a major role for ERα in gene regulation, tumorigenesis, metastatic progression, and TGF-β activity in BPTF<sup>KO</sup> mammary tumor cells.

# Pharmacologic BPTF inhibition restores ERα expression and blocks metastatic progression of mammary tumors

Given the development of potent, selective small molecule inhibitors targeting BPTF, we next assessed whether pharmacologic inhibition of BPTF could replicate the effects of its genetic deletion. We first characterized the effect of pre-treating 4T1 cells, a well-established hormone-negative murine mammary tumor cell line, with the selective BPTF inhibitor S-AU-1, which is more suitable for in vitro applications due to its short half-life<sup>46</sup>. To evaluate tumor growth dynamics, 4T1 cells were pre-treated S-AU-1 or DMSO as a control for 48 h prior to their transplantation into the mammary fatpad of immunocompetent Balb/C female mice. Treatment of 4T1 cells with S-AU-1 (5  $\mu$ M) for 48 h did not impact overall cell viability (Supplementary Fig. 9A). We found that transient inhibition of BPTF function via S-AU-1 pre-treatment significantly delayed the initial stages of mammary tumor growth, which normalized overtime to reach the same size of tumors from DMSO-treated 4T1 cells, thus corroborating the delayed tumor growth dynamics seen in the BPTFKO model (Supplementary Fig. 9B). To characterize the metastatic properties of 4T1 cells with BPTF inhibition, we performed a Transwell migration assay. With this assay, we observed a decrease in the abundance of 4T1 cells that migrated to the lower chamber in response to S-AU-1 pre-treatment compared to DMSO-treated 4T1 cells, suggesting the decreased migratory potential of BPTF<sup>KO</sup> tumor cells (Supplementary Fig. 9C).

We next evaluated whether inhibition of BPTF with S-AU-1 would result in the gain of ER $\alpha$  expression. To this end, we treated MMTV-PyMT tumor organoids and tumor organoids derived from the C3(1)-TAg model of mammary tumorigenesis with S-AU-1, and we observed an increase in increased *Esr1* mRNA and ER $\alpha$  protein levels

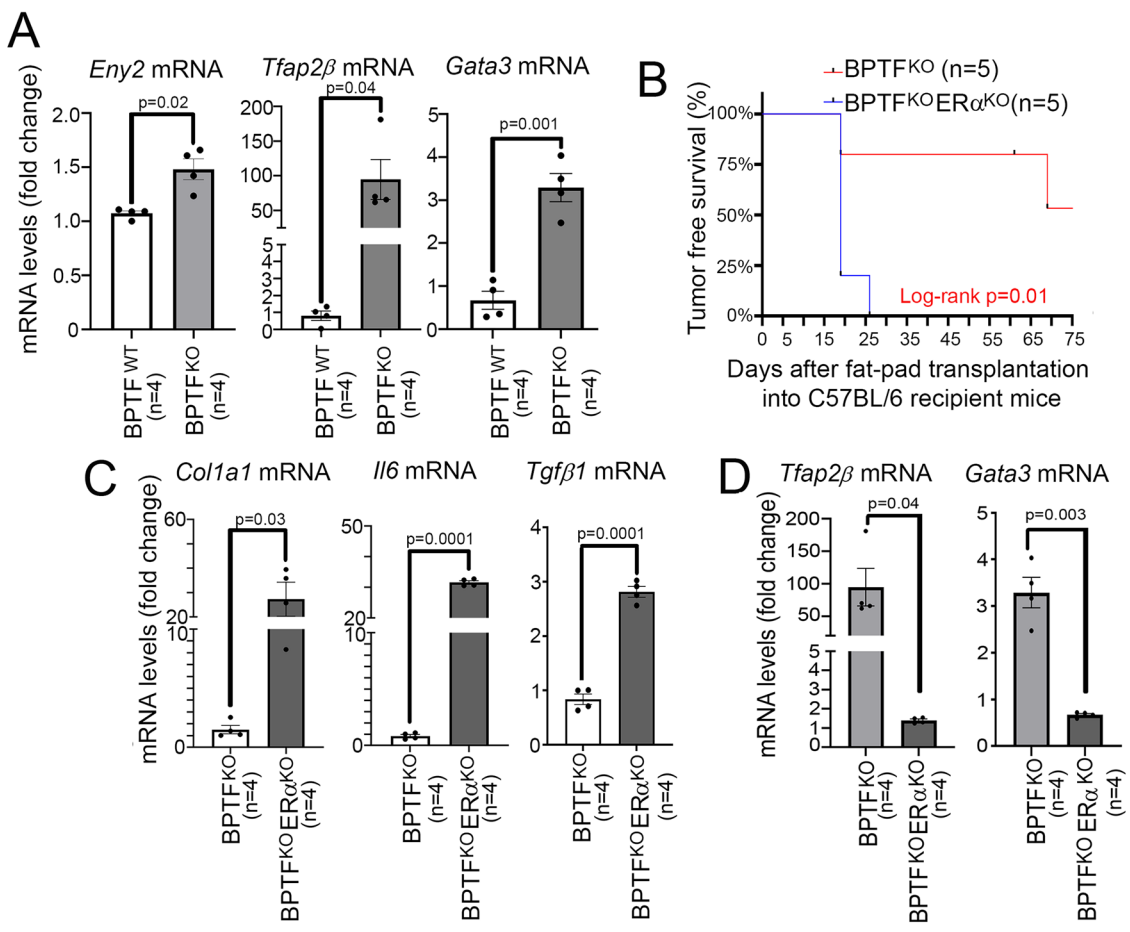


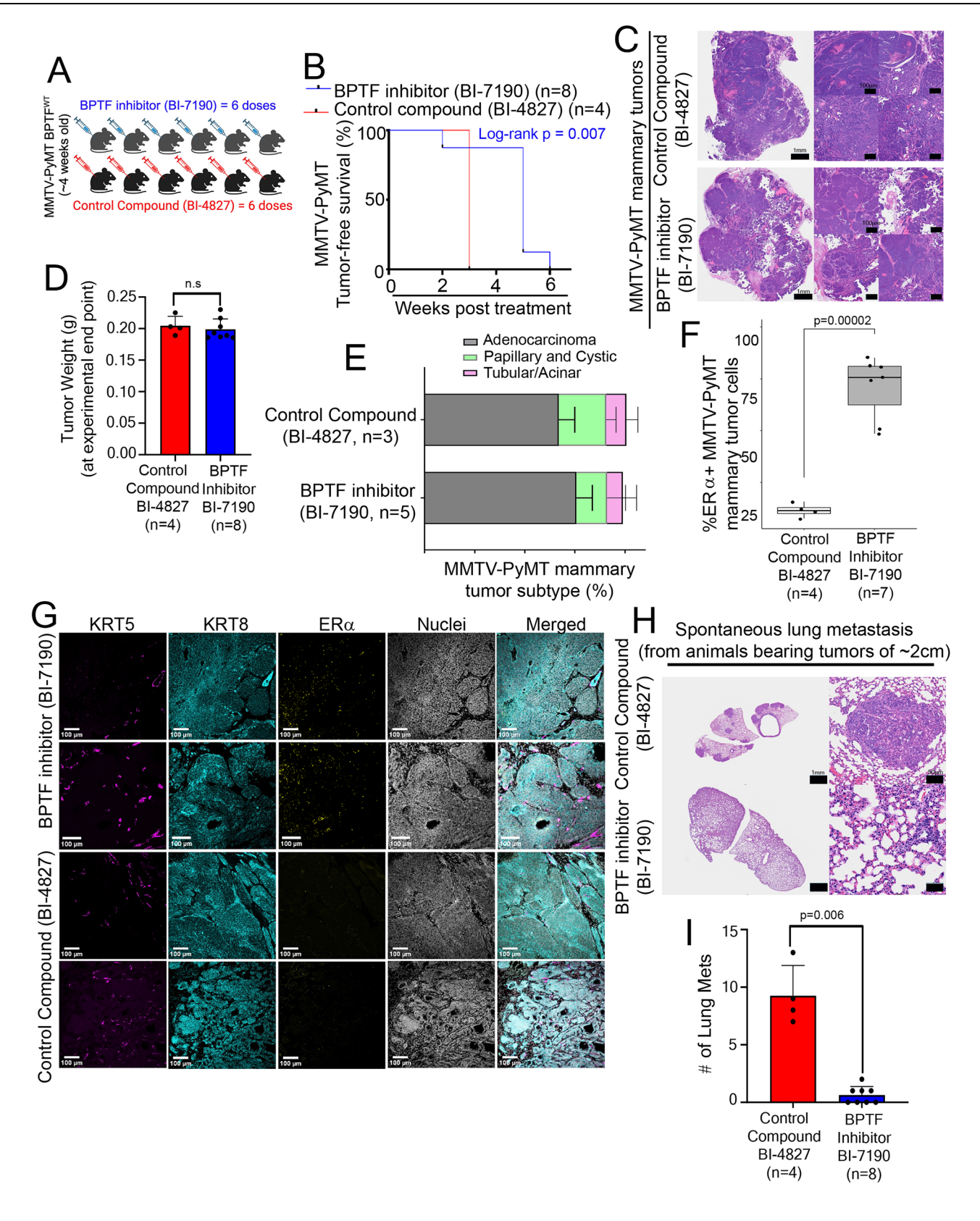
**Fig. 3** | **ERα** is the key regulator of tumorigenesis delay and metastatic suppression in BPTF<sup>KO</sup> mice. **A** qPCR quantification of Eny2, Tfap2β, and Gata3 mRNA levels in BPTF<sup>KO</sup> and BPTF<sup>KO</sup> mammary tumor organoids. n = 4 biological replicates. **B** Tumor-Free survival analysis of C57BL/6 female mice transplanted with BPTF<sup>KO</sup>/ERα<sup>KO</sup> (n = 5) mammary tumor organoids. Statistical analysis performed with Log-rank (Mantel–Cox) test. **C** qPCR quantification of Colla1, ll6 and Tgfβ1 mRNA levels in BPTF<sup>KO</sup>/ERα<sup>WT</sup> and BPTF<sup>KO</sup>/ERα<sup>KO</sup> mammary tumor

organoids. n = 4 biological replicates. **D** qPCR quantification of  $Tfap2\beta$  and Gata3 mRNA levels in MMTV-PyMT BPTF<sup>KO</sup>/ER $\alpha$ <sup>WT</sup> and BPTF<sup>KO</sup>/ER $\alpha$ <sup>KO</sup> tumor organoids. n = 4 biological replicates. Statistical analysis performed with an unpaired t-test with Welch's correction (two-sided), and significant differences were considered if p < 0.05. Error bars represent standard error mean. Samples (n) represent number of individual mice or number biological replicates. Source data and p values are provided as a Source Data file.

(Supplementary Fig. 9D, E and Supplementary Table 1). Increased ESR1 mRNA levels in response to S-AU-1 treatment were also observed in breast cancer organoids derived from TNBC invasive ductal carcinomas from two different patients, thus corroborating with our observations from mouse tumor cells and human cancer cell lines (Supplementary Fig. 9F, G and Supplementary Table 1). Interestingly, ESR1 mRNA levels remained unchanged in breast cancer organoid systems derived from ERα + PR+ invasive ductal carcinomas from two different patients treated with S-AU-1, indicating conditions that BPTF inhibition did not affect ER $\alpha$  expression in hormone-positive breast cancers (Supplementary Fig. 9H, I and Supplementary Table 1). It is worth noting that breast cancer cells are known to lose ERα expression when grown as organoids, raising the possibility that such culturing conditions result in caveats when studying the mechanistic action of BPTF inhibition. In fact, S-AU-1 treatment of patient-derived breast cancer organoid cultures increased the percentage of apoptotic cells across all conditions, a phenotype that was not exacerbated by cotreatment with TAM, thus suggesting that in these systems, BPTF inhibition strongly suppresses cell viability (Supplementary Fig. 9F-I).

To evaluate whether the gain of *ESR1* expression induced by treatment-induced BPTF inhibition was also linked with alterations in the chromatin landscape, we performed ATAC-seq to profile changes to chromatin accessibility of MCF-7 cells treated with the BPTF inhibitor, given that S-AU-1 treatment resulted in a three-fold increase of *ESR1* 

mRNA levels (Supplementary Fig. 10A; Supplementary Table 1 and 2). We first compared the datasets generated from S-AU-1 treated-MCF-7 cells to the datasets we generated from MCF-7 cells expressing BPTF sgRNA (Supplementary Fig. 7). Principal component analysis clustered the samples based on BPTF inhibition or control conditions, (PC1, 56.5% variation), suggesting that pharmacological targeting of BPTF yielded a similar landscape of chromatin accessibility (ATAC-seq peaks) compared to genetic targeting of BPTF, and that these regions were substantially different from control conditions (Supplementary Fig. 10B). Analysis of total ATAC-seq peaks indicated an expansion of accessible sites, specifically at intergenic and genic genomic regions, in cells treated with S-AU-1 (Supplementary Fig. 10C). This result resembled the previously reported effects of the genetic deletion of BPTF in normal mouse mammary epithelial cells, suggesting that BPTF inhibition allows for genomic accessibility specifically at distal regulatory regions<sup>13</sup>. Further analysis of the accessible regions and DEGs exclusive to the BPTF inhibitor treatment condition revealed upregulation of ERα downstream genes, including Solute Carrier family 17 member 11 (SLC7A11), Early Growth Response 1 (ERG1), Zinc Finger MYND-type containing 8 (ZMYND8), Fos proto-oncogene, AP1 transcription factor subunit (FOS), and Insulin-like growth factor-binding protein 3 (IGFBP3) (Supplementary Fig. 10D, E)52-55. Analysis of EREs showed a two-fold increase in ATAC-seq signal in response to BPTF inhibition, suggesting that the loss of BPTF function enhances chromatin accessibility at regions



canonically occupied by ER $\alpha$ , mirroring the results of our ATAC-seq analysis of MCF-7 cells expressing BPTF sgRNA (Supplementary Fig. 10F).

To directly test the effects of BPTF chemical inhibition in vivo, we utilized the recently developed selective BPTF inhibitor BI-7190<sup>56</sup> and characterized its effect on MMTV-PyMT mammary tumor development (Fig. 4A). Tumor-free survival analysis showed that nearly 100%

of mice treated with BPTF inhibitor remained tumor-free for approximately five weeks, in marked contrast to 100% of mice treated with the control compound that developed tumors within three weeks from the start of treatment (Fig. 4B). Yet, similar to the BPTF<sup>KO</sup> model, pharmacologic inhibition of BPTF did not impact the ability of mammary tumors to develop to their maximum size (2 cm), with similar tumor weight across conditions at experimental endpoint (Fig. 4C, D).

**Fig. 4** | **Pharmacologic BPTF inhibition restores ERα expression and blocks metastatic progression of mammary tumors. A** Experimental approach for oral gavage treatment of MMTV-PyMT mice with control compound BI-4827 (n = 4) or BPTF inhibitor BI-7190 (n = 8). Created in BioRender. Ciccone, M. (2025) https://BioRender.com/n1thfyz. **B** Tumor-free survival analysis of MMTV-PyMT mice treated with control compound BI-4827 (n = 4), or BPTF inhibitor BI-7190 (n = 8). Statistical analysis performed with Log-rank (Mantel–Cox) test. **C** H&E-stained histological images of experimental end point (-2 cm) mammary tumors from MMTV-PyMT treated with control compound BI-4827 (n = 4), or BPTF inhibitor BI-7190 (n = 8). Scale bar = 1 mm. Zoom-in panels, Scale bar = 50 μm. **D** Wet weight (in grams) of MMTV-PyMT mammary tumors from mice treated with control compound BI-4827 (n = 4 individual animals) or BPTF inhibitor BI-7190 (n = 8 individual animals) (tumors at experimental endpoint, -2 cm). **E** Histopathological classification of mammary tumors from MMTV-PyMT mice treated with control compound BI-4827 (n = 4 individual animals) or BPTF inhibitor BI-7190 (n = 8 individual

animals). Immunofluorescence (IF) quantification (F) and images (G) of percentage of ER $\alpha$ + mammary tumor cells (tumors at experimental endpoint, -2 cm) from MMTV-PyMT mice treated with control compound BI-4827 or BPTF inhibitor BI-7190 (n = 7). KRT5 (magenta), KRT8 (cyan), ER $\alpha$  (yellow), Nuclei (DAPI, gray). Scale bar = 100  $\mu$ m. H H&E-stained histological images from the lungs from tumorbearing MMTV-PyMT mice treated with Control compound BI-4827 or BPTF inhibitor BI-7190 (tumors at experimental endpoint, tumors -2 cm). Scale bar = 1 mm. Zoom-in panels, Scale bar = 50  $\mu$ m. I Quantification of the number of metastatic lung lesions in tumor-bearing MMTV-PyMT mice treated with control compound BI-4827 (n = 4) or BPTF inhibitor BI-7190 (n = 8) (tumors at experimental endpoint, tumors -2 cm). Statistical analysis performed with an unpaired t-test with Welch's correction, and significant differences were considered if p < 0.05. Error bars represent standard error mean. Samples (n) represent number of individual mice or number biological replicates. Source data and p values are provided as a Source Data file.

Histological analysis of endpoint mammary tumors demonstrated that mice treated with BPTF inhibitor BI-7190 and the control compound spanned histological subtypes commonly observed in the MMTV-PyMT model, thus validating that pharmacologic inhibition of BPTF did not alter the gross pathology of mammary tumors (Fig. 4E). IF analysis showed a three-fold increase of ER $\alpha$  expression in late-stage tumors from mice treated with BPTF inhibitor BI-7190, thus confirming that independent of the strategy of BPTF inhibition, loss of BPTF function results in the development of ERα+ mammary tumors (Fig. 4F, G). In fact, analysis of lungs from mice treated with BPTF inhibitor BI-7190 indicated a four-fold decrease in the number of lung metastases compared to mice treated with a control compound (Fig. 4H, I). Collectively, our data suggest that pharmacologic inhibition of BPTF mimics the effects of genetic deletion of BPTF observed ex vivo and in vivo. These results also validate that changing the epigenetic landscape of mammary tumor cells via BPTF inhibition is a promising strategy for activating ER $\alpha$  responses and suppressing the metastatic properties of cancer cells (Supplementary Fig. 10G).

#### Discussion

Perturbations to epigenetic homeostasis can lead to changes that result in aberrant gene expression and enable malignant cells to adapt and actively remodel their environment. These changes include abnormal cell growth, EMT, and alterations in stem cell potency, all of which can impact the cellular lineage hierarchy. Our previous work has demonstrated that BPTF plays a role in maintaining MaSC stemness and negatively regulating differentiation into the luminal lineage during normal mammary gland development<sup>13</sup>. Here, we expanded upon our original findings to establish a role for BPTF in negatively regulating the expression of the luminal lineage gene *Esr1* in mammary tumorigenesis. We also illustrate that genetic and chemical inhibition of BPTF alters the development, progression, and therapeutic sensitivity of murine and human breast cancer models.

Previous studies that pursued shRNA targeting of BPTF function using cancer cell lines in vivo showed a moderate effect on tumor growth  $^{20,57}$ , similar to what we observed in our studies. Concordantly, transiently targeting BPTF with small molecule chemical inhibitors also indicated moderate effects on tumor growth  $^{27,58}$ . However, considering the role of BPTF as a putative chromatin remodeler, none of these studies evaluated alterations in the molecular features of mammary tumors nor cancer progression as a result of targeting BPTF. Our study mechanistically dissected the previously uncharacterized molecular basis of such phenotypes; we show that the loss of BPTF, and the resultant chromatin remodeling, activates the expression of ER $\alpha$ , resulting in downstream inhibition of TGF- $\beta$  signaling and mammary oncogenesis.

Currently, DepMap resources classify BPTF as a common essential gene across several human cancer cell lines. However, the same database identifies elevated BPTF mRNA expression as a specific feature of

breast cancer compared to other solid tumors<sup>59</sup>. Interestingly, loss of BPTF in adult mice, under the regulation of the Krt5 promoter, a marker expressed in various epithelial and immune cell types, did not affect overall health or survival, thus arguing against a broader tissue-wide dependency on BPTF expression, at least in adult mice<sup>13</sup>. Our current research also demonstrates that treatment of adult mice with a selective BPTF inhibitor, which mimics the effects of genetic BPTF deletion on tumor growth, ERa expression, and metastatic progression, does not impact overall animal health. Instead, our findings indicate that BPTF loss only mildly affects mammary tumor growth, further challenging the conventional notion of BPTF pan-essentiality. Additionally, our studies have serendipitously identified BPTF deletion as a strategy for experimentally modeling ERα-positive mammary tumorigenesis. Although ERα-positive breast cancers represent the most prevalent subtype of breast cancer diagnosed in women, modeling ERα-positive mammary tumorigenesis has been a challenge, as most mouse models of mammary tumorigenesis are hormone-negative, lose expression of ERα, or do not depend on estrogen for their growth<sup>60</sup>.

Although experimental models targeting hormone-negative breast cancers with endocrine therapy have revealed intriguing but unclear mechanisms of non-canonical estrogen receptor-related pathways in regulating cellular growth, migration, and tumorigenesis, endocrine therapies have not become the standard of care for hormone-negative breast cancers. Gain of ERα functionality has long been perceived as a strategy that would create an opportunity for hormone targeting therapies to be used to treat hormone-negative breast cancer and breast cancers that have developed resistance to previous hormone therapies<sup>61-64</sup>. The challenge in restoring ERα expression in hormone-negative breast cancer subtypes is often due to epigenetic suppression of ESR1 expression, most notably through hypermethylation of the ESR1 promoter<sup>65</sup>. Using hormone-positive and hormone-negative models of human breast cancer, including endocrine-therapy resistant cell lines, we show that the loss of BPTF function induces the gain of functional ERa expression, restores molecular responses to estrogen, and sensitizes tumors to hormone targeting therapy. Consistent with this, genetic ablation of ERa in BPTF<sup>KO</sup> tumors reversed tumor growth kinetics, suppressed lung metastasis formation, and reprogrammed gene expression profiles, supporting a functional role for ERα as a key mediator of BPTF loss phenotypes. Therefore, our findings implicate BPTF inhibition as a promising strategy that may broaden the application of hormone therapies to hormone-negative and endocrine therapy-resistant breast cancers.

It is plausible that BPTF, through both its bromodomain regions, actively maintains an open chromatin state that sustains  $ER\alpha$  expression and transcriptional activity. As these cells progress through tumor development, BPTF-regulated nucleosome repositioning and the expression of additional TFs likely contribute to changes in chromatin accessibility, cellular state, and function. Thus, loss of BPTF in this

context likely prevents the loss of chromatin accessibility required to sustain ER $\alpha$  levels, which may be linked to aggressive tumor development and metastasis. In fact, this phenotype is recapitulated by ER $\alpha$  deletion alone, suggesting that BPTF-directed chromatin reorganization is critical for ER $\alpha$  expression regulation in mammary tumor cells. Our analysis of genetically engineered BPTF loss-of-function models (GEMMs and CRISPR-Cas9) revealed that targeting BPTF with small-molecule inhibitors that block its bromodomain yields similar phenotypes. These findings suggest that BPTF's bromodomain region mediates chromatin accessibility switches needed during tumor progression, including those that suppress ER $\alpha$  programs and activate TGF- $\beta$  programs, thus guiding transcriptional regulation that dictate aggressive cellular states.

Notably, previous analyses of normal MaSC, as well as current analysis of human cancer cell lines, suggest that BPTF loss or inhibition leads to gains of chromatin accessibility. In each case, the gain in accessibility was linked to increased activity of specific TFs, which guided changes to cellular states linked to stemness, and in this context, is driven by ERα. These observations also raise the possibility that, when in high abundance, specific lineage TFs could play a crucial role in occupying genomic regions, even in the absence of fully functional chromatin remodeling factors. Alternatively, the release of NURF complex components in the absence of BPTF may enable their integration into alternative chromatin remodeling complexes, thereby regulating cellular processes.

Independent of the initial hormone status, ~30% of all breast cancer cases will progress to metastatic disease, which is difficult to treat and negatively impacts patient survival<sup>66,67</sup>. Despite the many advances in combination therapy, patients with metastatic breast cancer still respond variably to treatments. This differential therapeutic response across different subtypes/grades of invasive disease represents a great clinically unmet need, demanding new strategies that will ensure consistent therapeutic efficacy<sup>68,69</sup>. Our findings suggest that quantifying BPTF mRNA levels in early breast cancer lesions may be a predictor of the likelihood of metastatic disease progression in breast cancer patients, providing a metric that can guide treatment plans. This may be particularly significant for patients with Ductal Carcinoma In Situ, a non-invasive subtype of breast cancer with the potential to progress to invasive and metastatic disease<sup>70</sup>. Our findings demonstrate that targeting BPTF in mice with pre-malignant mammary lesions, but prior to the detection of palpable tumor, significantly delayed the onset of mammary tumors and effectively blocked metastatic development. These results highlight a potential therapeutic window for targeting early-stage breast cancer, perhaps independent of hormone receptor status, offering a strategy that could enhance the efficacy of endocrine therapy and mitigate metastatic progression.

Importantly, our study reinforces the rationale for targeting BPTF as a therapeutic strategy to not only reduce metastatic spread but also enhance the efficacy of hormone therapies in breast cancer, including cases that are resistant to conventional treatments. Overall, our work also contributes to the expanding knowledge of chromatin dependencies and cell state dynamics in driving breast cancer initiation, progression, and as suitable strategies to improve responses to targeted therapies.

#### **Methods**

#### Animals

All animal experiments were conducted in accordance with approved protocols from the CSHL Institutional Animal Care and Use Committee (IACUC). Mice were maintained on a 12-h light/12-h dark cycle, at a controlled temperature of 72 °F and humidity ranging from 40–60%. MMTV-PyMT transgenic mice (C57BL/6 background), as well as C57BL/6 and NOD/SCID female mice, were obtained from The Jackson Laboratory and Charles River. The MMTV-PyMT *KrtS*<sup>CR-ERT2</sup>*Bptf*<sup>fl/fl</sup> (BPTF<sup>KO</sup>) strain was generated by crossing MMTV-PyMT transgenic mice with

 $KrtS^{CRE-ERT2}Bptf^{fift}$  mice. Similarly, the MMTV-PyMT  $KrtS^{CRE-ERT2}Bptf^{fift}Esr1^{fift}$  (BPTF<sup>KO</sup>ER $\alpha^{KO}$ ) strain was established by crossing MMTV-PyMT BPTF<sup>KO</sup> mice with  $Esr1^{fift}$  mice. Female mice ranging in age from 3 to 20 weeks were used for all experiments. Procedures, including mammary tumor monitoring, mammary fat pad transplantation, and treatments, are detailed in the Supplemental Experimental Procedures. For experiments involving tumor growth, the maximal tumor size allowed by CSHL IACUC is 2 cm, and this limit was strictly adhered to.

#### Mouse tamoxifen (TAM) treatment

To prepare the working solution, TAM powder (Sigma, Cat# T5648-1G) was weighed and initially dissolved in ethanol by vortexing. Heatsterilized sunflower oil (Sigma, Cat# S5007-250ML) was then added at a 19:1 oil-to-ethanol ratio to achieve a final concentration of 500 µg/ 100 μL (one dose). The mixture was heated to 55 °C and vigorously shaken to ensure homogeneity. For induction of BPTF deletion, transgenic female mice received 3 intraperitoneal injections of TAM (5 mg/kg) on alternate days. To induce deletion of both BPTF and ERα, MMTV-PyMT BPTF<sup>fl/fl</sup>Esr1<sup>fl/fl</sup> and BPTF<sup>fl/fl</sup>Esr1<sup>wt/wt</sup> mice were allowed to form tumors, which were subsequently harvested for organoid culture. After passaging, organoids were dissociated into single cells, and approximately 5 × 10<sup>5</sup> cells were injected into distal mammary fat pads. One-week post-transplant, mice were administered 3 additional intraperitoneal doses of TAM (5 mg/kg) on alternate days. For experiments assessing the anti-tumor effects of TAM, mice received daily intraperitoneal injections of 100 µg per day for 10 consecutive days.

#### **Antibodies**

All antibodies were purchased from companies as indicated below and used without further purification. Antibodies for lineage depletion: biotinylated anti-CD45 (Thermo Fisher Scientific Cat# 13-0451-85, RRID:AB 466447) (1:100 dilution), biotinylated anti-CD31 (Thermo Fisher Scientific Cat# 13-0311-85, RRID:AB 466421) (1:200 dilution), biotinylated anti-Ter119 (Thermo Fisher Scientific Cat# 13-5921-85. RRID:AB 466798) (1:200 dilution), and biotinylated anti-CD34 (Thermo Fisher Scientific Cat# 13-0341-82, RRID:AB 466425) (1:200 dilution). Antibodies for IF staining: Alexa Fluor 647 conjugated anti-Cytokeratin 5 - KRT5 - (Abcam, Cat# AB193895; RRID:AB 2728796) (1:300 dilution); Alexa Fluor® 488 anti-Cytokeratin 5-KRT5-(Abcam, Cat# ab193894, RRID:AB\_2893023) (1:300 dilution); Alexa Fluor 405 conjugated anti-Cytokeratin 8-KRT8-(Abcam, Cat# ab210139; RRID:AB\_ 2890924) (1:300 dilution), Alexa Fluor 546 Polyoma virus middle T antigen Antibody (Santa Cruz Biotechnology, Cat# sc-53481; RRID: AB\_ 630138) (1:50 dilution), N-cadherin (H-2) (Santa Cruz Biotechnology, Cat# sc-393933, RRID:AB 2832921) (1:300). Alexa Fluor 488 pSMAD (Bioss, Cat#bs-11641R-A488, RRID: AB\_3665803) (1:100 dilution), Alexa Fluor 488 BPTF/FALZ (Bioss, Cat# bs-11641R-A488, RRID:AB\_3665804) (1:300 dilution), Alexa Fluor 647 Estrogen Receptor alpha (H226) (Santa Cruz Biotechnology, Cat# sc-53493, RRID:AB 629461) (1:100 dilution). Antibodies for IHC: Rabbit anti-BPTF antibody (Bioss, Cat# bs-11641, RRID:AB 2938605) (1:100 dilution), Antibodies for Western Blot: mouse anti-β-Actin antibody (Santa Cruz Biotechnology Cat# sc-81178, RRID:AB 2223230) (1:5000 dilution), Rabbit anti-ERα antibody (Santa Cruz Biotechnology Cat# sc-544, RRID:AB\_631469) (1:300 dilution), goat anti-rabbit IgG HRP (Abcam Cat# ab6721, RRID:AB 955447) (1:10,000 dilution) and goat anti-mouse IgG HRP (Abcam Cat# ab97051, RRID:AB\_10679369) (1:20,000 dilution). Antibodies for Flow cytometry analysis: 7-AAD viability staining solution (BioLegend Cat# 420404, RRID:SCR 020993) (1:200 dilution), FITC con-jugated anti-CD3 (BioLegend Cat# 100204, RRID:AB 312661) (1:100 dilution), Alexa Fluor 700 conjugated. anti-NK1.1 (BioLegend Cat# 108730, RRI-D:AB 2291262) (1:100 dilution), Brilliant Violet 421 conjugated anti-CD206 (BioLegend Cat# 141717, RRID:AB 2562232) (1:100 dilution), Alexa Fluor 700 conjugated anti-Ly6G (BioLegend Cat# 127621,

RRID:AB\_10640452) (1:200 dilution), PE/Cyanine7 anti-mouse/human CD11b (BioLegend Cat# 101216, RRID:AB\_312799) (1:200 dilution), PE/Cyanine7 anti-mouse CD103 (BioLegend Cat# 121425, RRID:AB\_2563690) (1:100 dilution); APC/Cyanine7 anti-mouse CD11c (BioLegend Cat# 117324, RRID:AB\_830649) (1:100 dilution).

#### Histological analysis

For histological studies, left inguinal mammary gland, mammary tumor, lung, and/or liver was harvested from individual animal and was fixed overnight in 4% paraformaldehyde prior to paraffin embedding. Tissue sections were stained with Hematoxylin and Eosin (H&E) for conventional histological analysis. Whole-section mammary tumor H&E slides were imaged using an Aperio ePathology slide scanner (Leica Biosystems) with 40× objectives, and the percent areas of individual tumor subtypes (adenocarcinoma, papillary, tubular/acinar) were quantified using ImageJ-Fiji. Histopathological evaluation was performed by Dr. Wilkinson (mouse pathologist).

#### scRNA-seq library preparation and data analysis

Mammary gland tissue from ~7-weeks old BPTFWT and BPTFKO female mice with non-palpable tumors was mechanically dissociated as previously described<sup>71</sup>. Digested tissue was incubated with lineagedepletion antibodies (Ter119, CD31, CD45) and passed through MACS magnetic columns (Miltenyi Biotec Cat# 130-042-401)<sup>71</sup> to enrich for lineage-negative epithelial cells. These cells were used for scRNA-seq library preparation on the 10× Chromium platform, followed by sequencing on the NextSeq High Output SE75 (28x56x8). Reads from single-cell assay (14,531 total cells) were aligned to the mm10 genome using CellRanger v3.1.0 (10x Genomics) (Cell Ranger, RRID:SCR\_017344)<sup>72</sup>, and downstream analysis was performed in Seurat v4.1.1 (SEURAT, RRID:SCR\_007322)<sup>73</sup>. Cells with fewer than 200 or more than 6000 features, or with >15% mitochondrial content, were excluded. Genes expressed in fewer than 3 cells were also removed, and data were log-normalized. Post-filtering, 9694 BPTFWT cells and 4837 BPTF<sup>KO</sup> cells were retained. Principal component analysis (PCA) was performed using the top 2000 variable genes to determine significant components for clustering. Shared nearest neighbor graphs were constructed using the first 10 principal components, with a clustering resolution of 0.3. Epithelial cells were defined by expression of Epcam, Krt8, Krt18, Krt5, and Krt14 (cluster average expression > 2). Re-clustering epithelial populations with 10 dimensions at a resolution of 0.5 yielded 6952 BPTFWT cells and 3515 BPTFKO cells. Fibroblast populations from nulliparous or post-lactation involution mice were identified based on lack of Epcam (epithelial), Pecam1 (endothelial), and *Ptprc* (immune) expression and positive expression of *Sparc*<sup>74</sup>. Cells were classified into three major states according to previously defined marker genes. Population abundance differences between conditions were quantified using the Propeller function from the Speckle package<sup>32</sup>, with no statistically significant changes observed between BPTFWT and BPTFKO clusters. DEGs defining each cluster were identified using known cell type markers and the FindAllMarkers() function in Seurat, which applies the Wilcoxon Rank Sum test. Cell cycle scoring was performed using CellCycleScoring() with default Seurat gene lists. Cluster dendrograms were generated using Build-ClusterTree(), and visualization of differential gene expression was performed using FeaturePlot(), VlnPlot(), and DotPlot() functions. Global analysis of DEGs was conducted using Gene Set Enrichment Analysis (RRID:SCR\_003199)<sup>75</sup>.

#### Immunofluorescence (IF) and image analysis

Paraffin-embedded sections of mammary gland/tumor, lung, and liver were first deparaffinized using xylene (Sigma, Cat# 534056) and subsequently rehydrated. Antigen retrieval was then carried out in Trilogy solution (Cell Marque, Cat# 920P-10). Following this step, deparaffinized tissue slides or whole tissue samples were rinsed briefly (for

1 min) in 1× PBS and incubated in blocking buffer (10 mM Tris-HCl, pH 7.4: 100 mM MgCl<sub>2</sub>: 0.5% Tween-20: 10% FBS: 5% goat serum) for 4 h in a humidified chamber. Samples were then incubated overnight (16 h. 4 °C) with directly conjugated primary antibodies diluted in the same blocking buffer. After washing with PBS and blocking solution, nuclei were counterstained with DAPI (Sigma, Cat# 10236276001) for 10 min. Finally, slides were mounted using ProLong Glass Antifade Mountant (Invitrogen, Cat# P36980). Imaging was performed on Zeiss LSM780 and LSM710 confocal microscopes using Zen lite Blue edition software (ZEN Digital Imaging for Light Microscopy, RRID:SCR 013672, version 2.0.0.0). Image analysis was performed using Imagel-Fiji (v2.16.0). To measure nuclear enrichment of ERa, raw images were minimally processed to enhance DAPI signal clarity by applying a despeckle filter and removing background noise using the Subtract Background tool with a rolling ball radius of 10 px. Nuclear regions were identified through segmentation, using an adaptive thresholding method tailored to each image to ensure consistent delineation of nuclear boundaries. Integrated density (IntDen) values of ERa were measured within the segmented nuclear regions, which were then normalized across samples to account for inter-sample variability, using total fluorescence and a cutoff was applied to exclude background fluorescence. For whole tissue image processing, orthogonal projections of z-stacks were performed using ImageJ-Fiji (v2.16.0). For nuclear versus non-nuclear pSMAD enrichment quantification, nuclear pSMAD staining was identified by its overlap with DAPI signals, regardless of its overlap with the Krt8 staining pattern. Non-nuclear pSMAD staining was defined by its differential overlap with Krt8 signals (vs DAPI). Staining patterns were visually assessed using orthogonal projections of each image. The nuclear-to-cytoplasmic (Nuc/Cyto) ratio of pSMAD enrichment was calculated by dividing the total instances of nuclear staining by the total instances of cytoplasmic staining for each image. Box-andwhisker plots were generated, and statistical analyses were performed using R (v4.2).

#### Flow cytometry analysis

Spontaneous or transplanted mammary tumors were harvested and digested into single cells. Surface staining and flow cytometry analysis were conducted following the protocol previously described for mammary gland samples<sup>71,76</sup>. Flow cytometry analysis of the tumor samples was performed recording an average of 3–5 × 10<sup>5</sup> live cells (7-AAD negative) per sample. For cell analysis, Dual Fortessa II cell analyzer (BD Bioscience) or MACSQuant (Miltenyi Biotech) were utilized. Data analysis was performed using FlowJo (BD Bioscience). To assess spectral overlap between the chosen fluorophores, we used single color cell controls.

#### **Tissue array IHC**

Tissue microarray was originally purchase from purchased from US Biomax (current TissueArray.com). Breast cancer tissue array (BC081120e) and Normal breast tissue array (BN08013s) were stained with anti-BPTF antibody (1:200 dilution). IHC staining and slide scanning was performed by CSHL Histology core. IHC stained tissue array slides were scanned, and the quantification was performed using NIH ImageJ software. The analysis was based on the integrated density of the DAB channel, with background value subtracted. Graphs were generated using GraphPad Prism software.

#### Cell lines and cell culture

MCF-7, Hs578T, MCF7-TAM $^R$ , 4T1 and 293FT cell lines were cultured in DMEM (Gibco cat# 11995073) medium supplemented with 10% FBS (Corning, cat# 35-010-CV) and 1% Penicillin-Streptomycin (Gibco, cat# 15140122). HCC-1143 cell line was cultured in RPMI (Gibco cat# 61870127) medium supplemented with 10% FBS (Corning, cat# 35-010-CV) and 1% Penicillin-Streptomycin (Gibco, cat# 15140122). All cell lines were kept at 37 °C in a humidified incubator with 5% CO<sub>2</sub>.

Cell lines were mycoplasma negative, and validated by the CSHL cell culture facility.

#### S-AU-1 treatment

The mammary gland tumor organoids were cultured in Essential media for 6 days. Subsequently, they were treated with S-AU-1 (5  $\mu$ M) or a vehicle control, Dimethylsulfoxide (DMSO) (ATCC). MCF-7 cells were seeded at a density of 6.0  $\times$  10<sup>4</sup> cells/mL in 6-well plates using DMEM medium supplemented with 10% FBS and 1% Penicillin-Streptomycin. HCC-1143 cells were seeded at a density of 6.0  $\times$  10<sup>4</sup> cells/mL in 6-well plates using RPMI medium supplemented with 10% FBS and 1% Penicillin-Streptomycin. After overnight attachment, the cells were treated with either S-AU-1 (5  $\mu$ M) or DMSO. The medium containing S-AU-1 or DMSO was refreshed every 12 h over a total period of 72 h. 4T1 cells were seeded at a density of 1.0  $\times$  10<sup>5</sup> cells in 2 mL of DMEM supplemented with 10% FBS and 1% Penicillin-Streptomycin in 6-well plates. The cells were allowed to attach overnight and either DMSO or S-AU-1 (5  $\mu$ M) was added. Medium was refreshed with DMSO or S-AU-1 every 12 h over a total period of 48 h.

## Plasmid construction, sgRNA cloning and Lentiviral transduction

Human BPTF sgRNA (CGGTGTCAGAATTGGTACCA), and human RPA3 sgRNA (CCGGCGTTGATGCGCGACCT) $^{46}$  were sub-cloned into an all-in-one doxycycline inducible lentiviral vector LentiCRISPR v2 (TLCV2, Addgene, cat#87360). DNA oligos of the sgRNAs were cloned into backbones using a BsmBI restriction site. Lentivirus was produced in 293FT cells by transfecting plasmids with helper plasmids VSVG (Addgene Cat# 14888) and psPAX2 (Addgene, Cat#12260) using polyethylenimine (PEI 25000, Sigma Cat# 764582-1G) as previously described $^{77}$ . For lentivirus infection, target cells were mixed with the virus and  $4 \,\mu\text{g/mL}$  polybrene (Santa Cruz Biotechnology Cat# sc-134220), then centrifuged at 2500 rpm for 25 min in 6-well plates. Medium was exchanged at 24 h after infection, and then  $1 \,\mu\text{g/mL}$  puromycin (Invivogen Cat# ant-pr-1) was added for selection at 48 h after infection.

# Competition-based assay to measure cell growth defects caused by sgRNAs

Puromycin-selected cells were combined with parental cells in a 1:1 ratio, and then cultured with Doxycycline (DOX, Fisher Scientific, Cat# NC0424034) (1 $\mu$ g/mL) to induce the expression of Cas9 and EGFP. The percentage of cells positive for the specific sgRNA (identified by EGFP positivity) was monitored over a time course using a MACSQuant 10 (Miltenyi Biotec). To evaluate the effect of individual sgRNAs on cellular proliferation, the GFP% at each time point was normalized to the GFP% at the initial time point, allowing for a comparison of the reduction in sgRNA-positive cell populations.

#### Magic red caspase 3/7 activity assay/live dead violet

Human breast cancer cell lines, expressing TLCV2 with no sgRNA (referred to as Empty Vector) or a sgRNA targeting BPTF<sup>46</sup>, were plated into 6-well plates at  $3.0 \times 10^4$  cells/mL (2 mL cell solution per well). HCC-1143 cells were seeded in 6 wells at  $3.0 \times 10^4$  cells/mL (1 mL cell solution per mL). After overnight attachment, the MCF7 TAM<sup>R</sup> cells were treated with 1  $\mu$ M 4-OHT (Sigma cat# H7904), 1  $\mu$ g/mL DOX or both for 5 days. HCC-1143 cells were treated for 10 days under similar conditions. TNBC breast cancer organoids were grown as indicated below. Human breast cancer tumor organoid lines, NH85, DS126, NH48, and NH53 were treated for 72 h with DMSO, S-AU-1 (5  $\mu$ M), 4-OHT or S-AU-1 (5  $\mu$ M), and 4-OHT (1  $\mu$ M) for 72 h. Magic Red (Immunochemistry technologies Cat# 936) and Live dead violet (Thermo Scientific Cat# L34964) staining followed manufacturers protocol. Flow cytometry was performed on a MACSQuant 10 (Miltenyi Biotech) and analyzed on Flowlo v10. Magic Red and Live dead

violet staining followed manufacturers protocol. Flow cytometry was performed on a MACSQuant 10 (Miltenyi Biotech) and analyzed on Flowlo v10.

#### ATAC-seq library preparation and analysis

Nuclei from MCF-7 cells were isolated using a hypotonic lysis buffer and treated with Tn5 transposase (Nextera DNA Sample Preparation Kit, Illumina, Cat# FC-121-1031) to generate ATAC-seq libraries. Two biological replicates were prepared for each experimental condition. Libraries were barcoded and amplified following established protocols<sup>78</sup>, pooled, and sequenced on an Illumina NextSeg500 platform (76 bp, single-end mode). Sequencing reads were aligned to the human hg38 reference genome using Bowtie2 (RRID:SCR\_016368)<sup>79</sup>, and alignment files from biological replicates were combined. Enriched regions were identified using MACS2 (RRID:SCR\_013291)80 with parameters set to a tag size of 25 bp and a q value threshold of 1.0e-2. Peaks were annotated relative to the hg38 genome with HOMER (RRID:SCR 010881)81, and classified as promoter, intergenic, or genic (including 5'UTR, exons, introns, transcription termination sites, 3' UTR, ncRNA, miRNA, snoRNA, and rRNA). Overlap of genomic intervals was assessed using the UCSC Genome Browser (RRID:SCR 005780)82 combination with the BEDTools intersect function (RRID:SCR\_006646)83; any base-pair overlap was considered shared, while non-overlapping regions were categorized as condition-specific. Venn diagrams were generated using the online tool available at https://www.meta-chart.com/venn. For estrogen response element (ERE) analysis, publicly available ER ChIP-seq datasets (ChIP-Atlas: ERX008575, ERX008617; ENCODE Project: ENCSR560BUE) were intersected with ATAC-seq peaks, and ERE signal intensities were compared across experimental conditions.

#### **Bulk RNA-seq library preparation and analysis**

Nuclei were isolated from MCF-7 cells treated with DMSO or S-AU-1 (5 µM) and homogenized in TRIzol LS (Thermo Fisher Scientific, Cat# 10296010) for RNA extraction. Double-stranded cDNA synthesis and Illumina library preparation were performed using the Ovation RNAseq System V2 (Nugen Technologies, Cat#7102-32), followed by library construction with the Ovation Ultralow DR Multiplex System (Nugen Technologies, Cat# 0331-32). Each library (n = 2 biological replicates per condition) was barcoded with Illumina TruSeq adapters to enable multiplexing and sequenced on an Illumina NextSeq500 with 76 bp single-end reads. Data quality control and preprocessing were performed using FastQC (RRID:SCR\_014583)84 and Trimmomatic (RRID:SCR\_011848)85 for sequence trimming. Reads were aligned to the reference genome using STAR (RRID:SCR 004463)86, and gene-level read assignment was conducted with **FeatureCounts** (RRID:SCR\_012919)87. Differential gene expression analysis across multiple conditions and replicates was performed using DESeq2 (RRID:SCR 000154) replicates<sup>88</sup>. Genes with p < 0.05 were considered statistically significant.

#### Mouse tumor organoid culture

Primary mammary tumors (experimental end point, -2 cm) were minced and subjected to a digestion process using 20 mL of AdDF + ++ medium (Advanced DMEM/F12 Thermo Scientific, Cat# 12634028, 5 mM GlutaMax Thermo Scientific Cat# 35050061, 5 mM HEPES Thermo Scientific, Cat# 15630080, 1% Penicillin/Streptomycin Thermo Fisher Scientific, Cat# 15140122) supplemented with 1 mg/mL Collagenase type IV (Sigma, Cat# C5138) for approximately 40 min at a 37 °C shaker. The fully digested solution was passed through a 100  $\mu$ m cell strainer (Falcon, Cat# 352360) to obtain a strained solution. The strained solution was washed with 10 mL of AdDF + ++ medium and then pulse centrifuged three times at 500 g to enrich for mammary tumor organoids. The organoids were manually counted, and they were plated at a density of approximately 2 organoids per  $\mu$ l in Matrigel

(Corning, Cat# 354230) or Collagen I (Corning, Cat# 354236). Each well was seeded with approximately 100 tumor organoids. After polymerization at 37 °C for 30 min,  $600\,\mu$ l of organoid culture medium (AdDF+++, 1X ITS-G) (Thermo Fisher Scientific, Cat#41400045), 2.5 nM recombinant murine FGF-basic (PeproTech, Cat#450-33) was added to each well. The organoids were then cultured at 37 °C in a humidified incubator with 5% CO<sub>2</sub>.

#### TGF-β1 ELISA

To prepare tumor lysates for TGF- $\beta$ 1 ELISA assay (Invitrogen, Cat# BMS608-4), mammary tumors from BPTFWT and BPTFKO were digested to single cells and centrifuged for 5 min at 500 x g. Tumor cell pellets was resuspended in 10 mL of RIPA Lysis Buffer (Santa Cruz Biotechnology, Cat# sc-24948) and incubated on ice for 30 min. The lysates were centrifuged for 5 min at 500 x g. Supernatant was prepared for the assay according to manufacturer's protocol. To prepare cell media for TGF- $\beta$ 1 ELISA, BPTFWT and BPTFKO mammary tumor organoids were cultured for 6 days. Media was then replaced with 1 mL of fresh media and incubated for 48 h before harvesting and centrifuging for 5 min at 500 x g. Cell media was prepared for the assay according to manufacturer's protocol. Tumor lysates and cell media, for each sample, were assayed in duplicate and reported as an average. Colorimetric readouts were obtained using a Perkin Elmer Enspire multimode plate reader.

#### qPCR analysis

Organoid cultures were first washed with 0.5 mL of PBS, followed by the addition of 0.5 mL of Trizol directly into each well containing organoids in Matrigel. Trizol was pipetted up and down until the organoids were no longer visible (approximately 10 times). Cell lines were washed with 1 mL PBS and followed by the addition of 1 mL of Trizol. RNA extraction was then performed using Phenol Chloroform. Subsequently, cDNA synthesis was carried out using the SuperScript IV<sup>TM</sup> kit (Thermo Fisher Scientific, Cat# 18091050). RT-qPCR was performed using a Quantstudio 6 instrument with SYBR Green Master mix (Applied Biosystems, Cat# 4368577). Each gene was quantified in at least duplicate. The relative gene expression was calculated using the delta-delta CT method, where the expression levels were normalized to the housekeeping gene,  $\beta$ -actin mRNA. Graphs were generated using GraphPad software. Primer sequences are provided on Supplementary Information File.

#### Patient-derived TNBC breast cancer organoids

Patient-derived breast organoid cultures were established by Dr. David Spector's group and maintained in Matrigel (Corning, Cat# 354230) domes. Organoids were cultured in medium supplemented with 10% R-Spondin1 conditioned medium, 5 nM Neuregulin 1 (Peprotech, 100-03), 5 ng/mL FGF7 (Peprotech, 100-19), 20 ng/mL FGF10 (Peprotech, 100-26), 5 ng/mL EGF (Peprotech, AF-100-15), 100 ng/mL Noggin (Peprotech, 120-10 C), 500 nM A83-01 (Tocris, 2939), 5  $\mu$ M Y-27632 (Abmole, Y-27632), 500 nM SB202190 (Sigma, S7067), 1× B27 supplement (Gibco, 17504-44), 1.25 mM N-acetylcysteine (Sigma, A9165), 5 mM nicotinamide (Sigma, N0636), and 50  $\mu$ g/mL Primocin (Invitrogen, ant-pm-1) in ADF+++ media. Fresh organoid culture medium was added every 3 days, and organoids were passaged every 3–5 days to prevent over-confluency.

#### Western blot

Organoid samples were lysed in 1× Laemmli buffer (Bio-Rad, Cat# 1610747) and resolved by electrophoresis on in-house prepared 10% SDS-PAGE gels. Proteins were transferred to PVDF membranes (Bio-Rad, Cat# 162-0177) using a wet-transfer system. Membranes were blocked in 1% BSA and incubated overnight at 4 °C with primary antibodies diluted in blocking buffer, followed by a 40 min incubation with HRP-conjugated secondary antibodies. Chemiluminescent detection

was performed using Luminata Crescendo Western HRP substrate (Millipore, Cat# WBLUR0100), and signals were visualized on autoradiography film (Lab Scientific, Cat# XARALF2025). Films were digitized using an Epson Perfection 2450 photo scanner.

#### **Organoid treatment**

Established BPTF<sup>WT</sup> and BPTF<sup>KO</sup> mammary tumor organoids were grown for 6 days with organoid media, then treated with the following conditions: TGF- $\beta$ 1 treatment: On day 6 of culture, mammary tumor organoids were treated with TGF- $\beta$ 1 (2 ng/mL, BioLegend, cat# 763102), or control condition, for 48 h. Bright-field images of treated and untreated organoids were captured to compare morphology and cell protrusions. TAM treatment. On day 6 of culture, mammary tumor organoids were treated with 4-OHT (1 μM, Sigma-Aldrich, cat# H7904) or vehicle control (EtOH) for 10 days. Brightfield images were captured to compare morphology and organoids size quantification. *17-β*-Estradiol treatment. On day 6, mammary tumor organoids were cultured without FGF-2 for 24 h. Organoids were then treated with 66.6 ng/mL 17-β-Estradiol (Sigma #E275), or 2.5 nM FGF-2, for 48 h. Bright-field images were captured to compare organoid size.

#### Mouse organoid culture on collagen

Primary mammary tumors from TAM treated BPTF<sup>KT</sup> and BPTF<sup>KO</sup> female mice (experimental end point, ~2 cm) were cultured on 50 µl collagen I (Corning cat# 354236) coated domes. On day 6 of culture, the organoids were subjected to treatment with TGF- $\beta$ 1 (2 ng/mL, BioLegend, cat# 763102), or IL-1 $\beta$  (10 ng/mL, BioLegend, cat# 575102), or TNF $\alpha$  (20 ng/mL, BioLegend, cat# 575202) for 48 h. Bright-field images of treated and untreated organoids were captured to compare morphology and cell protrusions.

#### Transwell invasion assay

Transwell inserts for 24-well plate (pore size 8 µm, Corning, cat# CLS3464) were coated with 75 µL of diluted growth factor reduced Matrigel (1:12 dilution with DMEM for 4T1 cells, 1:7 dilution with AdDF + ++ for MMTV-PvMT mammary tumor organoids) and allowed to polymerize at 37 °C for 1 h. 4T1 cells, treated with either DMSO or S-AU-1 (5  $\mu$ M) for 48 h, were seeded at a density of 1 × 10<sup>5</sup> cells per well in 0.5 mL of serum-free DMEM supplemented with 1% Penicillin-Streptomycin in the upper chamber of a Transwell insert. 0.5 mL DMEM supplemented with 10% FBS and 1% Penicillin Streptomycin was added to the lower chamber. For cells derived from organoids,  $5 \times 10^5$ cells in 0.5 mL of organoid culture medium were added to the upper chamber. In the lower chamber, 0.75 mL of organoid culture medium containing 5% FBS was added. The cells were allowed to migrate along the serum gradient for 24 h. Cells were then fixed with cold methanol and stained with 1% crystal violet. Wells were then washed three times with distilled water and cells remain in upper chamber were removed with a cotton applicator. Images of 5 regions of interest on each insert membrane were acquired on a Leica microscope equipped with a camera (need to add microscope and camera details) using the 10× objective. Migrated cells were counted manually.

#### 3D Matrigel drop invasion assay

BPTF<sup>WT</sup> and BPTF<sup>KO</sup> mammary tumor organoids were harvested and digested into single cells. The cell number and viability were assessed using trypan blue staining. The cells were then resuspended in cold organoid culture medium to a final density of  $10^6$  cells per mL and mixed in a 1:1 ratio with neutralized Collagen I (3 mg/mL) on ice. A  $10~\mu$ L droplet of the cell mixture, containing approximately 5000 cells, was placed in the center of each well in a 24-well plate, forming a drop-like shape. The Collagen I drop was allowed to solidify at 37 °C in a humi-dified incubator with 5% CO<sub>2</sub> for 30 min. After solidification, 0.5 mL of organoid culture medium containing 5% FBS was added to each well. Phase-contrast images were captured to evaluate the invasion and

migration capabilities of the cells. Subsequently, the cell-collagen drops were fixed with 4% PFA and stained with 1% crystal violet, followed by washing with PBS. The area occupied by spreading cells was quantified using NIH Imagel software.

# Wholemount immunofluorescence (IF) of mammary tumor organoids

To prepare organoids for IF staining and imaging, cultures were disassociated with 500 µL of Matrigel Melting Solution (Cold Spring Harbor Laboratory Organoid Core) for 30 min at 4 °C followed by centrifugation at 500 x g in a 1% BSA (diluted in 1× PBS, Gibco cat #A10008-01) coated 15 mL conical tube. The supernatant was removed, and the organoid pellet was resuspended in 4% Paraformaldehyde (diluted in 1× PBS, Electron Microscopy Sciences, cat# 15711) for 1 h at room temperature. Fixed organoids were incubated with 1 mL of permeabilization (0.5% Triton X-100, Sigma cat# 93443 in 1× PBS) and incubated at room temperature for 30 min. Following a 5 min 500 x g spin, the fixed and permeabilized organoids were washed with PBST (0.1% Tween-20 solution, MP, cat# 9005-64-5 in 1X PBS) and incubated with 500 µL of blocking buffer (1X PBS 300 mM Glycine, Fischer-Scientific, cat# G45-212; 10 mg/mL BSA, Sigma cat# A2153; 5% Goat serum, Abcam cat# ab7481) at room temperature for 1 h. Blocked organoids were then stained overnight in blocking buffer containing indicated concentrations of indicated antibodies with constant agitation. Stained organoids were washed with 1× PBST and centrifuged for 5 min at 500 x g 3 times. All supernatant was removed, and 1 drop of Prolong™ Glass Antifade Mountant (Invitrogen cat #P36982) was added to the organoids followed by mounting on a glass slide with a coverslip before curing overnight in the dark at room temperature. Imaging was acquired on a Zeiss 710 or 780 Confocal Microscope.

#### NOD/SCID mammary fatpad transplantation

Mammary tumors (-2 cm in diameter) harvested from MMTV-PyMT *Bptf*<sup>fl/fl</sup> (non-TAM treated) female mice<sup>71</sup>, and enriched mammary tumor epithelial cells via depletion (TerI19, CD31, CD34, and CD45) of blood cells, endothelial cells, fibroblasts, and immune cells.  $5 \times 10^5$  tumor epithelial cells were transplanted into the mammary gland fatpad of nulliparous NOD/SCID female mice. Transplanted mice (day 7 post-transplant) were treated with intraperitoneal injections of sunflower oil (BPTFWT) or TAM (BPTFKO) 3 doses every other day. Tumor size was tracked beginning at the appearance of a palpable lesion up to 45 days. Volumes of tumors were determined by measuring each tumors length and width using a 6" digital caliper (Pittsburg, cat# BOOCM8YYKO).

# C57BL/6 mammary fatpad transplantation and tamoxifen administration

Mammary tumors (-2 cm in diameter) harvested from MMTV-PyMT  $Bptf^{\text{fl/fl}}$  (non-TAM treated) female mice<sup>71</sup>, and enriched mammary tumor epithelial cells via depletion (Ter119, CD31, CD34, and CD45) of blood cells, endothelial cells and fibroblasts.  $5 \times 10^5$  tumor epithelial cells were transplanted into the mammary gland fatpad of nulliparous C57BL/6 female mice. Starting from day 7 post-transplantation, the mice received daily intraperitoneal TAM injections of  $100 \, \mu\text{g/day}$  until they were euthanized. Tumor size was tracked from day 21 post-transplantation. Volumes of tumors were determined by measuring each tumors length and width using a 6" digital caliper (Pittsburg, cat# BOOCM8YYKO).

#### Tail vein injection of tumor organoids

MMTV-PyMT mammary tumor organoids were harvested and digested into single cells and cell clusters. For each genotype, a 1:1 mixture of cells from two different mice was used. Approximately  $1\times 10^6$  tumor epithelial cells in 100  $\mu$ l of PBS were injected into each mouse via tailvein injection. Lungs from these mice were collected five weeks from

the date of injection and examined for tumor metastases. The left lungs were homogenized in Trizol, and RNA was extracted to assess PyMT expression using qPCR. The right lungs were fixed in 4% PFA for histological analysis.

#### 4T1 orthotopic injection and tumor measurement

4T1 cells, pre-treated with DMSO or S-AU-1  $(5\,\mu M)^{13}$  for 48 h, were resuspended with 50% growth factor reduced Matrigel solution and injected in each inguinal mammary fat pad of 10-week-old nulliparous Balb/c female mice  $(5\times 10^4$  cells per injection). Once palpable tumors were detected, tumor volumes were calculated by measuring the length and width of tumors twice a week using a 6" digital caliper (Pittsburg, cat# BOOCM8YYKO). Mice were euthanized when tumors reached ~2 cm (humane endpoint).

#### **BPTF inhibitor BI-7190 treatment**

For oral gavage, either BI-7190 (BPTF inhibitor, Boehringer Ingelheim) or BI-4827 (Control compound, Boehringer Ingelheim) were dissolved into 0.5% Hydroxyethyl-cellulose (Sigma Cat# 09368-100 G) via sonication to a final concentration of 4.5 mg/mL. BPTF<sup>WT</sup> MMTV-PyMT mice (-10 weeks old, without palpable tumor) were treated with BPTF inhibitor or Control compound 3 times a week (30 mg/kg in 100 µl per dose, via gavage). Tumor growth was monitored twice a week, and animals were euthanized when tumor reached experimental end point (-2 cm).

#### Statistical analysis

Statistical analysis and graphs were generated using the GraphPad Prism software (GraphPad Software Inc, San Diego, CA). For all statistical analysis, error bars indicate standard error of mean across samples of the same experimental group. Nonparametric unpaired t tests, Log-rank (Mantel-Cox) tests, and Welch's t-test were used as indicated on figure legend. Samples (n) represent number of individual mice or number independent biological replicates. Raw data and p values are provided as a Source Data file.

#### **Reporting summary**

Further information on research design is available in the Nature Portfolio Reporting Summary linked to this article.

#### **Data availability**

scRNA-seq, ATAC-seq, and RNA-seq, datasets were deposited into BioProject database under number PRJNA973067, as bellow indicated. All sequencing data is publicly available. All accession numbers are listed on Supplementary Table 2. This manuscript does not report original code. Source data are provided with this paper.

#### References

- Kaur, J., Daoud, A. & Eblen, S. T. Targeting chromatin remodeling for cancer therapy. Curr. Mol. Pharm. 12, 215–229 (2019).
- Yomtoubian, S. et al. Inhibition of EZH2 catalytic activity selectively targets a metastatic subpopulation in triple-negative breast cancer. Cell Rep. 30, 755–770.e6 (2020).
- Kurani, H. et al. DOT1L is a novel cancer stem cell target for triple-negative breast cancer. Clin. Cancer Res. 28, 1948–1965 (2022).
- Schade, A. et al. Abstract P4-08-11: AKT and EZH2 inhibitors kill TNBCs by hijacking mechanisms of involution. *Cancer Res.* 83, P4-08-11 (2023).
- Hart, C. et al. Challenges in the management of advanced, ERpositive, HER2-negative breast cancer. Nat. Rev. Clin. Oncol. 12, 541–552 (2015).
- Will, M., Liang, J., Metcalfe, C. & Chandarlapaty, S. Therapeutic resistance to anti-oestrogen therapy in breast cancer. *Nat. Rev. Cancer.* 23, 673–685 (2023).

- Garcia-Martinez, L., Zhang, Y., Nakata, Y., Chan, H. L. & Morey, L. Epigenetic mechanisms in breast cancer therapy and resistance. Nat. Commun. 12, 1786 (2021).
- Feng, Q. et al. An epigenomic approach to therapy for tamoxifenresistant breast cancer. Cell Res. 24, 809–819 (2014).
- Landry, J. et al. Essential role of chromatin remodeling protein bptf in early mouse embryos and embryonic stem cells. *PLoS Genet.* 4, e1000241 (2008).
- Xiao, H. et al. Dual functions of largest NURF subunit NURF301 in nucleosome sliding and transcription factor interactions. *Mol. Cell* 8, 531–543 (2001).
- Radzisheuskaya, A. et al. An alternative NURF complex sustains acute myeloid leukemia by regulating the accessibility of insulator regions. EMBO J. 42, e114221 (2023).
- Richart, L. et al. BPTF is required for c-MYC transcriptional activity and in vivo tumorigenesis. *Nat. Commun.* 7, 10153 (2016).
- Frey, W. D. et al. BPTF maintains chromatin accessibility and the self-renewal capacity of mammary gland stem cells. Stem Cell Rep. 9, 23–31 (2017).
- Mayes, K. et al. BPTF depletion enhances T-cell-mediated antitumor immunity. Cancer Res. 76, 6183–6192 (2016).
- Sinanian, M. M. et al. A BPTF inhibitor that interferes with the multidrug resistance pump to sensitize murine triple-negative breast cancer cells to chemotherapy. *Int. J. Mol. Sci.* 25, 11346 (2024).
- Wagner, K. U., Ward, T., Davis, B., Wiseman, R. & Hennighausen, L. Spatial and temporal expression of the Cre gene under the control of the MMTV-LTR in different lines of transgenic mice. *Transgenic* Res. 10, 545–553 (2001).
- Shishido, S., Delahaye, A., Beck, A. & Nguyen, T. A. The MMTV-PyVT transgenic mouse as a multistage model for mammary carcinoma and the efficacy of antineoplastic treatment. J. Cancer Ther. **04**, 1187–1197 (2013).
- Ito, I. et al. Estrogen inhibits transforming growth factor β signaling by promoting Smad2/3 degradation. J. Biol. Chem. 285, 14747–14755 (2010).
- Ariazi, E. A. et al. A new role for ERα: silencing via DNA methylation of basal, stem cell, and EMT genes. Mol. Cancer Res. 15, 152–164 (2017).
- Bezrookove, V. et al. BPTF promotes the progression of distinct subtypes of breast cancer and is a therapeutic target. Front. Oncol. 12, 1011173 (2022).
- Curtis, C. et al. The genomic and transcriptomic architecture of 2,000 breast tumours reveals novel subgroups. *Nature* 486, 346–352 (2012).
- Pereira, B. et al. The somatic mutation profiles of 2,433 breast cancers refines their genomic and transcriptomic landscapes. *Nat. Commun.* 7, 11479 (2016).
- Rueda, O. M. et al. Dynamics of breast-cancer relapse reveal laterecurring ER-positive genomic subgroups. *Nature* 567, 399–404 (2019).
- 24. Lefebvre, C. et al. Mutational profile of metastatic breast cancers: a retrospective analysis. *PLoS Med.* **13**, e1002201 (2016).
- Liu, J. et al. An integrated TCGA pan-cancer clinical data resource to drive high-quality survival outcome analytics. *Cell* 173, 400–416.e11 (2018).
- Zahid, H. et al. New design rules for developing potent cell-active inhibitors of the nucleosome remodeling factor (NURF) via BPTF bromodomain inhibition. J. Med. Chem. 64, 13902–13917 (2021).
- Gao, S., Zhang, W., Ma, J. & Ni, X. PHF6 recruits BPTF to promote HIF-dependent pathway and progression in YAP-high breast cancer. J. Transl. Med. 21, 220 (2023).
- 28. Gonzalez, H., Hagerling, C. & Werb, Z. Roles of the immune system in cancer: from tumor initiation to metastatic progression. *Genes Dev.* **32**, 1267–1284 (2018).
- 29. Kos, K. & De Visser, K. E. The multifaceted role of regulatory T cells in breast cancer. *Ann. Rev. Cancer Biol.* **5**, 291–310 (2020).

- Mayes, K. et al. BPTF inhibits NK cell activity and the abundance of natural cytotoxicity receptor co-ligands. Oncotarget 8, 64344–64357 (2017).
- Henry, S. et al. Characterization of gene expression signatures for the identification of cellular heterogeneity in the developing mammary gland. J. Mammary Gland Biol. Neoplasia 26, 43–66 (2021).
- 32. Phipson, B. et al. propeller: testing for differences in cell type proportions in single cell data. *Bioinformatics* **38**, 4720–4726 (2022).
- Lin, E. Y. et al. Progression to malignancy in the polyoma middle T oncoprotein mouse breast cancer model provides a reliable model for human diseases. Am. J. Pathol. 163, 2113–2126 (2003).
- 34. Ortiz, J. R. et al. Single-cell transcription mapping of murine and human mammary organoids responses to female hormones. *J. Mammary Gland Biol. Neoplasia* **29**, 3 (2024).
- 35. Shishido, S., Delahaye, A., Beck, A. & Nguyen, T. A. The MMTV-PyVT Transgenic mouse as a multistage model for mammary carcinoma and the efficacy of antineoplastic treatment. *J. Cancer Ther.* **4**, 11 (2013).
- 36. Fares, J., Fares, M. Y., Khachfe, H. H., Salhab, H. A. & Fares, Y. Molecular principles of metastasis: a hallmark of cancer revisited. Signal Transduct. Target. Ther. **5**, 28 (2020).
- Kim, R. S. et al. Dormancy signatures and metastasis in estrogen receptor positive and negative breast cancer. PLoS ONE 7, e35569 (2012).
- Chatterjee, S. J. & McCaffrey, L. Emerging role of cell polarity proteins in breast cancer progression and metastasis. *Breast Cancer.* 6, 15–27 (2014).
- von Locquenghien, M., Rozalén, C. & Celià-Terrassa, T. Interferons in cancer immunoediting: sculpting metastasis and immunotherapy response. J. Clin. Investig. 131, 143296 (2021).
- 40. Ye, X. et al. Upholding a role for EMT in breast cancer metastasis. *Nature* **547**, E1–E3 (2017).
- 41. Massagué, J. TGFbeta in cancer. Cell 134, 215-230 (2008).
- Katsuno, Y., Lamouille, S. & Derynck, R. TGF-β signaling and epithelial-mesenchymal transition in cancer progression. *Curr. Opin. Oncol.* 25, 76–84 (2013).
- Derynck, R., Turley, S. J. & Akhurst, R. J. TGFβ biology in cancer progression and immunotherapy. *Nat. Rev. Clin. Oncol.* 18, 9–34 (2021).
- Eyre, R. et al. Microenvironmental IL1beta promotes breast cancer metastatic colonisation in the bone via activation of Wnt signalling. *Nat. Commun.* 10, 5016 (2019).
- 45. Wolczyk, D. et al. TNF- $\alpha$  promotes breast cancer cell migration and enhances the concentration of membrane-associated proteases in lipid rafts. *Cell. Oncol.* **39**, 353–363 (2016).
- Kirberger, S. E. et al. Selectivity, ligand deconstruction, and cellular activity analysis of a BPTF bromodomain inhibitor. *Org. Biomol. Chem.* 17, 2020–2027 (2019).
- 47. Hens, J. et al. Analysis of gene expression in PTHrP-/- mammary buds supports a role for BMP signaling and MMP2 in the initiation of ductal morphogenesis. *Dev. Dyn.* **238**, 2713–2724 (2009).
- Kang, H. J. et al. Differential regulation of estrogen receptor a expression in breast cancer cells by metastasis-associated protein 1. Cancer Res. 74, 1484–1494 (2014).
- Hoch, R. V., Thompson, D. A., Baker, R. J. & Weigel, R. J. GATA-3 is expressed in association with estrogen receptor in breast cancer. *Int. J. Cancer* 84, 122–128 (1999).
- Wu, M. V. & Tollkuhn, J. Estrogen receptor alpha is required in GABAergic, but not glutamatergic, neurons to masculinize behavior. Horm. Behav. 95, 3–12 (2017).
- Green, J. E. et al. The C3(1)/SV40 T-antigen transgenic mouse model of mammary cancer: ductal epithelial cell targeting with multistage progression to carcinoma. *Oncogene* 19, 1020–1027 (2000).

- Li, C., Harada, A. & Oh, Y. IGFBP-3 sensitizes antiestrogen-resistant breast cancer cells through interaction with GRP78. Cancer Lett. 325, 200–206 (2012).
- 53. Liu, R. et al. The dual regulation effects of ESR1/NEDD4L on SLC7A11 in breast cancer under ionizing radiation. *Front. Cell Dev. Biol.* **9**, 772380 (2022).
- Farcas, A. M., Nagarajan, S., Cosulich, S. & Carroll, J. S. Genomewide estrogen receptor activity in breast cancer. *Endocrinology* 162, bqaa224 (2021).
- 55. Kim, H. R. et al. Egr1 is rapidly and transiently induced by estrogen and bisphenol A via activation of nuclear estrogen receptor-dependent ERK1/2 pathway in the uterus. *Reprod. Toxicol.* **50**, 60–67 (2014).
- Martinelli, P. et al. Discovery of a chemical probe to study implications of BPTF bromodomain inhibition in cellular and in vivo experiments. ChemMedChem 18, e202200686 (2023).
- Dar, A. A. et al. The role of BPTF in melanoma progression and in response to BRAF-targeted therapy. J. Natl. Cancer Inst. 107, div034 (2015).
- 58. Tyutyunyk-Massey, L. et al. Autophagy-dependent sensitization of triple-negative breast cancer models to topoisomerase II poisons by inhibition of the nucleosome remodeling factor. *Mol. Cancer Res.* **19**, 1338–1349 (2021).
- Tsherniak, A. et al. Defining a cancer dependency map. Cell 170, 564–576.e16 (2017).
- Dabydeen, S. A. & Furth, P. A. Genetically engineered ERα-positive breast cancer mouse models. *Endocr Relat. Cancer* 21, R195–R208 (2014).
- Sharma, D., Saxena, N. K., Davidson, N. E. & Vertino, P. M. Restoration of tamoxifen sensitivity in estrogen receptor-negative breast cancer cells: tamoxifen-bound reactivated ER recruits distinctve corepressor complexes. *Cancer Res.* 66, 6370–6378 (2006).
- Fan, J. et al. ERα negative breast cancer cells restore response to endocrine therapy by combination treatment with both HDAC inhibitor and DNMT inhibitor. J. Cancer Res. Clin. Oncol. 134, 883–890 (2008).
- Hostetter, C. L., Licata, L. A. & Keen, J. C. Timing is everything: Order of administration of 5-aza 2' deoxycytidine, trichostatin A and tamoxifen changes estrogen receptor mRNA expression and cell sensitivity. *Cancer Lett.* 275, 178–184 (2009).
- Zhang, X. et al. Mechanisms of Gefitinib-mediated reversal of tamoxifen resistance in MCF-7 breast cancer cells by inducing ERα re-expression. Sci. Rep. 5, 7835 (2015).
- 65. Martínez-Galán, J. et al. ESR1 gene promoter region methylation in free circulating DNA and its correlation with estrogen receptor protein expression in tumor tissue in breast cancer patients. *BMC Cancer* **14**, 59 (2014).
- Wang, H. et al. The prognosis analysis of different metastasis pattern in patients with different breast cancer subtypes: a SEER based study. Oncotarget 8, 26368–26379 (2017).
- 67. Wang, R. et al. The Clinicopathological features and survival outcomes of patients with different metastatic sites in stage IV breast cancer. *BMC Cancer* **19**, 1091 (2019).
- 68. Johansson, A. L. V. et al. In modern times, how important are breast cancer stage, grade and receptor subtype for survival: a population-based cohort study. *Breast Cancer Res.* **23**, 17 (2021).
- Nolan, E., Lindeman, G. J. & Visvader, J. E. Deciphering breast cancer: from biology to the clinic. Cell 186, 1708–1728 (2023).
- Shehata, M. et al. Ductal carcinoma in situ: current concepts in biology, imaging, and treatment. J. Breast Imaging 1, 166–176 (2019).
- Dos Santos, C. O. et al. Molecular hierarchy of mammary differentiation yields refined markers of mammary stem cells. *Proc. Natl. Acad. Sci. USA* https://doi.org/10.1073/pnas.1303919110 (2013).

- 72. Zheng, G. X. Y. et al. Massively parallel digital transcriptional profiling of single cells. *Nat. Commun.* **8**, 14049 (2017).
- Stuart, T. et al. Comprehensive integration of single-cell data. Cell 177, 1888–1902.e21 (2019).
- 74. Henry, S. et al. Host response during unresolved urinary tract infection alters female mammary tissue homeostasis through collagen deposition and TIMP1. *Nat. Commun.* **15**, 3282 (2024).
- Subramanian, A. et al. Gene set enrichment analysis: a knowledge-based approach for interpreting genome-wide expression profiles. *Proc. Natl. Acad. Sci. USA* https://doi.org/10.1073/pnas. 0506580102 (2005).
- Hanasoge Somasundara, A. V. et al. Parity-induced changes to mammary epithelial cells control NKT cell expansion and mammary oncogenesis. Cell Rep. 37, 110099 (2021).
- 77. Wu, X. S. et al. OCA-T1 and OCA-T2 are coactivators of POU2F3 in the tuft cell lineage. *Nature* **607**, 169–175 (2022).
- Buenrostro, J. D., Giresi, P. G., Zaba, L. C., Chang, H. Y. & Greenleaf, W. J. Transposition of native chromatin for fast and sensitive epigenomic profiling of open chromatin, DNA-binding proteins and nucleosome position. *Nat. Methods* https://doi.org/10.1038/nmeth. 2688 (2013).
- Langmead, B., Trapnell, C., Pop, M. & Salzberg, S. L. Ultrafast and memory-efficient alignment of short DNA sequences to the human genome. *Genome Biol.* https://doi.org/10.1186/gb-2009-10-3r25 (2009).
- 80. Zhang, Y. et al. Model-based analysis of ChIP-Seq (MACS). Genome Biol. https://doi.org/10.1186/gb-2008-9-9-r137 (2008).
- Benner, C., Heinz, S. & Glass, C. K. HOMER Software for motif discovery and next generation sequencing analysis. http://homer. ucsd.edu/homer/ (2017).
- 82. Dreszer, T. R. et al. The UCSC genome browser database: extensions and updates 2011. *Nucleic Acids Res.* **40**, D918–D923 (2012).
- Quinlan, A. R. & Hall, I. M. BEDTools: a flexible suite of utilities for comparing genomic features. *Bioinformatics* https://doi.org/10. 1093/bioinformatics/btq033 (2010).
- 84. Andrews, S. FASTQC a quality control tool for high throughput sequence data. Babraham Institute (2015).
- 85. Bolger, A. M., Lohse, M. & Usadel, B. Trimmomatic: a flexible trimmer for Illumina sequence data. *Bioinformatics* https://doi.org/10.1093/bioinformatics/btu170 (2014).
- Dobin, A. et al. STAR: ultrafast universal RNA-seq aligner. Bioinformatics 29, 15–21 (2013).
- 87. Liao, Y., Smyth, G. K. & Shi, W. FeatureCounts: an efficient general purpose program for assigning sequence reads to genomic features. *Bioinformatics* https://doi.org/10.1093/bioinformatics/btt656 (2014).
- 88. Anders, S. & Huber, W. Differential expression analysis for sequence count data. *Genome Biol.* **11**, R106 (2010).

#### **Acknowledgements**

This work was performed with assistance from CSHL Animal Facility, the CSHL Tissue Histology Shared Resources, the CSHL NextGen Sequencing Shared Resources, the CSHL Single Cell Shared Resources, the CSHL Flow Cytometry Shared Resources, and the CSHL Microscopy Shared Resources, which are supported by the CSHL Cancer Center Support Grant 5P30CA045508. This work was financially supported by the Pershing Square Sohn Prize for Cancer Research (C.O.D.S.), the CSHL and Simons Foundation Award (C.O.D.S.), the CSHL and Northwell Health affiliation (C.O.D.S.), the NIH/NCI grant R01CA248158-01 (C.O.D.S.), NIH/NIA grant R01 AG069727-01 (C.O.D.S.), the NIH/NCI R01CA284630 (C.O.D.S.), and the NIH MIRA award R35GM140837-02 (W.C.K.P.).

#### **Author contributions**

C.O.D.S. designed and supervised the research; C.O.D.S. and D.A. wrote the manuscript. C.O.D.S., M.F.C., D.C., D.A., C.C., S.M.L, M.C., C.Z.Z., S.T.Y., S.R., and A.V.H.S., performed experiments and analyzed results. M.C.T., R.A., and Y.Z. performed computational analyses. W.C.K.P., J.O., D.L.S., and J.T. provided essential reagents. A.S. provided critical feedback. J.E.W. performed histopathological analysis.

#### **Competing interests**

The authors declare no competing interests.

#### **Additional information**

**Supplementary information** The online version contains supplementary material available at https://doi.org/10.1038/s41467-025-64255-8.

**Correspondence** and requests for materials should be addressed to Camila O. dos Santos.

**Peer review information** *Nature Communications* thanks the anonymous reviewer(s) for their contribution to the peer review of this work. A peer review file is available.

Reprints and permissions information is available at http://www.nature.com/reprints

**Publisher's note** Springer Nature remains neutral with regard to jurisdictional claims in published maps and institutional affiliations.

Open Access This article is licensed under a Creative Commons Attribution-NonCommercial-NoDerivatives 4.0 International License, which permits any non-commercial use, sharing, distribution and reproduction in any medium or format, as long as you give appropriate credit to the original author(s) and the source, provide a link to the Creative Commons licence, and indicate if you modified the licensed material. You do not have permission under this licence to share adapted material derived from this article or parts of it. The images or other third party material in this article are included in the article's Creative Commons licence, unless indicated otherwise in a credit line to the material. If material is not included in the article's Creative Commons licence and your intended use is not permitted by statutory regulation or exceeds the permitted use, you will need to obtain permission directly from the copyright holder. To view a copy of this licence, visit http://creativecommons.org/licenses/by-nc-nd/4.0/.

© The Author(s) 2025